INFORMATION TO USERS

This manuscript has been reproduced from the microfilm master. UMI films the text directly from the original or copy submitted. Thus, some thesis and dissertation copies are in typewriter face, while others may be from any type of computer printer.

The quality of this reproduction is dependent upon the quality of the copy submitted. Broken or indistinct print, colored or poor quality illustrations and photographs, print bleedthrough, substandard margins, and improper alignment can adversely affect reproduction.

In the unlikely event that the author did not send UMI a complete manuscript and there are missing pages, these will be noted. Also, if unauthorized copyright material had to be removed, a note will indicate the deletion.

Oversize materials (e.g., maps, drawings, charts) are reproduced by sectioning the original, beginning at the upper left-hand corner and continuing from left to right in equal sections with small overlaps.

Photographs included in the original manuscript have been reproduced xerographically in this copy. Higher quality 6" x 9" black and white photographic prints are available for any photographs or illustrations appearing in this copy for an additional charge. Contact UMI directly to order.

Bell & Howell Information and Learning
300 North Zeeb Road, Ann Arbor, MI 48106-1346 USA
800-521-0600

UMI®

Use of 3D Deformable Models for Intraoperative Visualization and Quantification of Cerebral Tissue Resection

Master's Thesis

Michael John Sinasac

Student ID: 9446681

Department of Electrical and Computer Engineering
Faculty of Engineering
McGill University
Montreal, Quebec, Canada

A Thesis submitted to the Faculty of Graduate Studies and Research in partial fulfillment of the requirements for the degree of Master of Engineering.

Contents

List of Figures

List of Tables

Acknowledgments

I wish to thank the following individuals for their help and support throughout the course of this thesis:

- Dr. Tim McInerney and Dr. Dimitri Terzopoulos of the University of Toronto for initial discussions regarding deformable models and sample code
- Roch Comeau, for a myriad of discussions on all aspects of medical imaging and other subjects and for his idea for the calibration of the aspirator simulator
- Michel Audette, for many not overwhelmingly 'unpleasant' discussions, both professional and personal and translating my abstract into french
- Reza Kasrai, Philippe St. Jean, Martin Cyr and Diego Clonda (and Roch and Michel again) for discussions, programming help, suggestions and being a great group of guys to work with
- Brad Gill for assisting me in the MR scan of the MR phantom for the mock resection trial
- Patrice Munger, for assistance with the gelatin phantoms and use of his phantom simulator software
- Rick Hoge, for suggestions on the construction of an MR phantom
- Eric Johnstone for his help on the aspirator simulator and MR phantom and use of the Biomedical Engineering workshop
- David McDonald, for assistance with his DISPLAY software
- Dr. Funnell, for his discussions on finite element issues and volume estimation
- NSERC for the financial support of a PGS A Scholarship
- my supervisor, Dr. Terry Peters, for his support and encouragement throughout my thesis, keeping in touch with me throughout my illness and recovery and for financial support during final months of my thesis
- to God, for granting me the opportunity to live to finish this thesis, for the patience, determination and iron will required to complete it, and for each day forward

I wish to dedicate this thesis to my father, John Sinasac, who passed away during the course of this work.

Abstract

The evolution of the various neuroimaging modalities and the use of computers in neurosurgery have provided the neurosurgeon with an ever increasing array of tools to use in treating the patient. Image guided neurosurgical systems, utilizing a computer display of multimodality preoperative images and some form of tracking device, allow the surgeon to navigate simultaneously in the real and computer worlds in order to plan trajectories, pinpoint locations of pathologies and to avoid areas of vasculature and vital brain function. These advances have served to improve outcomes and enhance productivity through improving conventional neurosurgical practices and allowing for the creation of new procedures which are made possible through enhanced visualization and manipulation of a patient's medical data. Intraoperatively however, the information provided by these systems becomes somewhat lacking after surgical procedures have been initiated since preoperative images are employed. Various intraoperative imaging techniques have been developed to provide feedback during the course of the surgical procedure. Although these techniques indeed furnish useful additional information, they often suffer from the drawbacks of being prohibitively expensive and can require specially designed operating theatres and specialized instruments to be used. In addition, the work of the surgeon is altered and/or interrupted using these intraoperative imaging techniques. The purpose of the project described in this thesis is to provide intraoperative feedback to the neurosurgeon using the equipment comprising a typical IGNS environment. The project accomplishes this task through the use of physically based, deformable models. The major objectives for this mode of intraoperative feedback are to provide useful visual and quantitative feedback to the neurosurgeon about the progress of tissue resection during a surgical procedure using the equipment available in a typical IGNS environment and to be simultaneously being unobtrusive to the surgeon's work.

An overview of the current state of IGNS is presented, followed by a logical association between current work and the significance of the project developed for this thesis. The mathematics of deformable models as a means for providing intraoperative feedback are developed and a thorough description of the work completed for this thesis is presented. A series of increasingly realistic validation studies that were undertaken for the

project are described, followed by a discussion of the use of the software in intraoperative applications. Finally, conclusions are made as to the utility of the project as a viable means of providing intraoperative feedback and future work is extrapolated from the project.

Resume

L'évolution des diverses modalités en imagerie neurologique ainsi que l'utilisation des ordinateurs pour la neurochirurgie ont fourni au (à la) chirurgien(ne) une vaste gamme d'outils pour traiter le patient. Les systèmes de neurochirurgie guidée par images (NCGI), mettant a profit l'affichage par écran cathodique des images multimodales préopératoires ainsi qu'un pointeur suivi en temps réel, permettent au chirurgien de naviguer simultanément dans les espaces réel et informatique, pour planifier les trajectoires, localiser les pathologies et éviter les endroits vitaux d'ordre vasculaire ou fonctionnel. Ces développements ont servi à améliorer les résultats des interventions ainsi que la productivité du chirurgien, par l'entremise du perfectionnement des procédures conventionnelles et de la création de nouvelles techniques exploitant la visualisation et la manipulation améliorées des données médicales du patient.

Toutefois, l'information fournie par ces systèmes peut devenir désuète, compte tenu de la nature préopératoire des images, une fois la procédure chirurgicale entamée. Pour parer à ce problème, quelques techniques d'acquisition d'images intraopératoires ont vu le jour, permettant la mise à jour du système pendant le cours d'une intervention. Même si ces techniques fournissent de l'information pertinente, leur application est limitée par leur coût prohibitif et parfois par les modifications qu'elles requièrent au niveau de la salle d'opération et des instruments chirurgicaux. De plus, le travail du chirurgien peut souvent être interrompu et/ou modifié en raison de ces techniques intraopératoires. L'objectif de ce projet de maîtrise est donc de fournir une rétroaction intraopératoire au neurochirurgien, en exploitant l'équipement habituel d'un système de NCGI. Le projet accomplit cette tâche par l'entremise de modèles physiques déformables de surface. Les contraintes les plus importantes de ce projet sont d'offrir une rétroaction visuelle et quantitative au chirurgien pendant l'intervention en exploitant l'équipement existant, tout en n'obstruant pas son travail.

Un survol de l'état actuel de la NCGI est présenté, suivi du liens entre cet environnement et le projet développé dans le cadre de cette thèse. Les mathématiques des modèles déformables comme technique de rétroaction intraopératoire sont développées et une description détaillée du travail qui sous-tend cette thèse y apparaît. Une série d'études

de validation qui fut effectuée dans le cadre du projet est décrite, suivie d'une discussion sur l'emploi clinique du logiciel. Enfin, nous tirons des conclusions vis-à-vis de l'utilité du projet en tant que source viable de rétroaction opératoire, et nous abordons les perspectives de travail futur.

List of Symbols and Abbreviations

2D	two dimensional
3D	three dimensional
AVM	arterio-venous malformation
BIC	Brain Imaging Center
CT	Computed Tomography
CSF	Cerebro-spinal Fluid
DSA	Digital Subtraction Angiography
EEG	Electroencephalography
FDA	Food and Drug Administration
FEA	Finite Element Analysis
FEM	Finite Element Modelling
fMRI	Functional Magnetic Resonance Imaging
GUI	graphical user interface
HPM	Homologous Point Matching
IGNS	Image Guided Neurosurgery
LED	light emitting diode
MEG	Magneto-encephalography
MHz	Mega hertz frequency unit
MIP	Maximum Intensity Projection
MNI	Montreal Neurological Institute
MRA	Magnetic Resonance Angiography
MR	Magnetic Resonance
MRI	Magnetic Resonance Imaging
NURBs	Non-uniform rational b-splines
OBT	Olivier-Bertrand-Tipal Stereotactic Frame
OR	operating room
PC	personal computer
PET	Positron Emission Tomography
RF	radio frequency

SGI	Silicon Graphics, Inc
TOF	time of flight
US	ultrasound
VIPER	Visualization Platform for Enhanced Reality

Chapter 1

Introduction

1.1 Overview of Image Guided Neurosurgery (IGNS)

The evolution of the various neuroimaging modalities and the use of computers in neurosurgery has provided the neurosurgeon with an ever increasing array of tools to use in treating the patient. Image guided neurosurgical systems, utilizing a computer display of multimodality preoperative images and some form of tracking device, allow the surgeon to navigate simultaneously in the real and computer worlds in order to plan trajectories, pinpoint locations of pathologies and to avoid areas of vasculature and vital brain function. These advances have served to improve outcomes and enhance productivity through improving conventional neurosurgical practices and allowing for the creation of new procedures which are made possible through enhanced visualization and manipulation of a patient's medical data [1]. Intraoperatively however, the information provided by these systems becomes somewhat lacking after surgical procedures have been initiated since preoperative images are employed. Various intraoperative imaging techniques have been developed to provide feedback during the course of the surgical procedure. Although these techniques indeed furnish useful additional information, they often suffer from the drawbacks of being prohibitively expensive and can require specially designed operating theatres and specialized instruments to be used. In addition, the work of the surgeon is altered and/or interrupted using these intraoperative imaging techniques. The focus of the work detailed in this thesis is to provide relevant intraoperative feedback using an existing image guided neurosurgical system while concurrently remaining unobtrusive to the surgeon's work.

1.2 Project Motivation

The following subsections briefly discuss the current state of IGNS with respect to the information provided to the neurosurgeon and thus provide the impetus for the undertaking of this project.

1.2.1 Use of Preoperative Images for Preoperative Planning and Intraoperative Navigation

Prior to a surgical procedure, the patient undergoes a series of medical imaging examinations in order to ascertain precisely the pathology that exists. These may serve to visually corroborate a preliminary diagnosis initially made by an analysis of symptoms and a physical neurological examination or the imaging studies may reveal an abnormality previously unforeseen. There are a wide range of imaging modalities at the surgeon's disposal and he/she may specify those modalities which target specific aspects of the patient's anatomy or physiology, such as those which visualize the white and grey matter of the brain, those which visualize the vasculature and those which focus on function related activity.

The imaging studies that are performed preoperatively are then used for surgical planning and some are ultimately used in the operating theatre for intraoperative guidance. The use of a computer display of preoperative images and a precision tracking device to relate a surgeon's position in the real world to his/her relative position in the virtual world of the imaging data sets is termed *frameless stereotactic surgery*. The basic premise of frameless stereotactic surgery is to allow the surgeon to precisely navigate through the patient's anatomy and locate the pathology while simultaneously avoiding vasculature and areas of vital brain function. A complete discussion of this type of surgery is presented in Chapter 2.

1.2.2 Limitations of the Use Preoperative Images Intraoperatively

The imaging studies performed prior to the surgical procedure serve as a road map for the neurosurgeon to safely find his/her way to the site of the pathology. A significant point to be made, however, is the fact that once the surgical procedure is underway the

accuracy of the preoperative images is degraded by a variety of factors. Effects such as pressure changes in the intracranial cavity upon opening the skull, tissue resection carried out during the course of the surgery and the effects of gravity are a few of the major influences that serve to produce deviations between the preoperative images on the computer display and the anatomy that the surgeon is dealing with. The issue of accuracy in IGNS is elucidated in Chapter 2. It should be noted that the focus of the project detailed in this thesis is to provide visual and quantitative feedback on the state of tissue resection during the course of the surgical procedure and not to correct for degradation of the preoperative images. This task is the subject of ongoing research in our laboratory [2,3].

1.2.3 The Need for Intraoperative Feedback

During the course of many surgical procedures tissue is resected. The preoperative images that are used for neurosurgical navigation do not reflect the changes made to the patient's anatomy and therefore the surgeon must mentally visualize what he/she has done and the extent of resection that has been performed. The aim of this project is to superimpose the changes made to the anatomy of the patient over the preoperative images to allow the surgeon to more easily visualize them. Updating of the preoperative images themselves to the current state of the patient's anatomy is the subject of ongoing work in our laboratory [2,3].

A secondary aim of the project is to allow for the visualization of the changes made to the patient's anatomy using the standard suite of tools currently available for frameless stereotactic interventions. That is, no additional specialized equipment is required such as ultrasound or more exotic technologies such as open coil MRI and specialized surgical instruments.

1.3 Intraoperative Neurosurgical Navigation

The following section gives a brief overview of the major facets comprising a frameless stereotactic neurosurgical environment. This is the environment around which the project was developed.

1.3.1 Computer Display of Preoperative Images

The display of preoperative images serves as the surgeon's virtual world in which he/she can navigate. Such a display is usually comprised of the three standard orientations: sagittal, coronal and axial (or transverse). These orientations are well known to neurologists and neurosurgeons from their historical use in radiographic studies. In addition to these three two dimensional (2D) images, the use of a three dimensional (3D) image (usually a surface rendering produced from the preoperative imaging data sets) is commonly added to provide further information on how the 2D images couple together in a 3D view of the anatomy. An example of a navigational display taken from VIPER (Visualization Platform for Enhanced Reality), a neurosurgical planning and navigation platform developed in our laboratory at the Montreal Neurological Institute (MNI) is shown in *Figure 1.1*.

Figure 1.1. A typical computer display used for IGNS.

1.3.2 Position Tracking Devices

In order for the surgeon to effectively use a computer display of preoperative images to plan a surgical approach and navigate through the patient's anatomy, some means of providing positional information relating the real and virtual worlds is necessary. Position tracking devices utilizing various technologies fulfill this need. These devices

allow the surgeon to pinpoint a location on the patient's anatomy and see the corresponding point as a crosshair position marker on the computer display of the 2D images and as a computer generated probe representation superimposed on the 3D image. The position tracking device used at the MNI is the FARO Surgicom (FARO Medical Technologies, Orlando, Fla), a six degree of freedom articulated arm, shown in *Figure 1.2*. A discussion of position tracking devices is presented in Chapter 2.

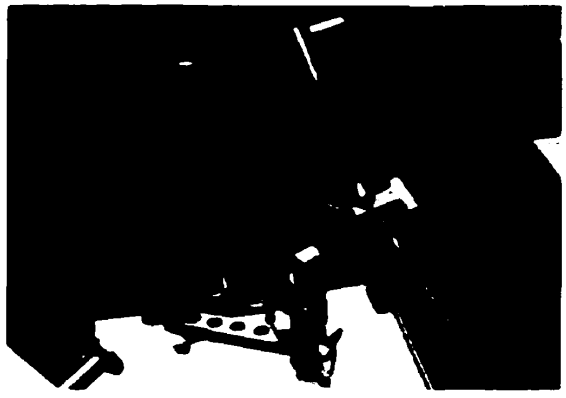

Figure 1.2. The FARO Surgicom Position Tracking Arm.

1.4 Current Neurosurgical Techniques for Intraoperative Feedback

Techniques for providing intraoperative feedback exist in the literature and are used primarily at research centers. The bulk of these techniques provide useful information to the neurosurgeon but often require extensive specialized and sometimes extremely expensive equipment in order to be used. Furthermore, many of these techniques fundamentally alter the course of the surgery in order to be carried out.

This section provides a survey of various alternatives for intraoperative feedback to contrast with the solution proposed in this project. A detailed explanation of the imaging modalities used in IGNS is presented in Chapter 2.

1.4.1 Anatomical

The use of computer assisted tomography (CT) systems intraoperatively was first proposed by Lunsford [4-6]. The surgical environment consisted of adjacent rooms: one

containing the OR suite and the other containing a CT scanner. This relatively early method allowed for the acquisition of intraoperative data but suffered from the disadvantages of subjecting the patient to radiation, having a fixed slice orientation and reduced soft tissue contrast relative to MRI [7]. Efforts therefore turned to developing an MR scanner capable of providing intraoperative feedback.

The use of magnetic resonance (MR) imaging is fundamental to IGNS. It is used extensively at the MNI for visualization and differentiation of soft tissue types and preoperative MR images are an integral part of the computer display used by the surgeon to navigate through the patient's anatomy. Recently, the use of MR scanners in the intraoperative environment has been proposed. A dedicated intraoperative MR scanner utilizing the GE SIGNA SP (0.5T field strength, double-torus design) has been described and used in a variety of neurosurgical interventions in [8]. The unique geometry of the MR scanner itself (a double vertical torus design allowing the surgeon to work between the magnets and use IGNS visualization and guidance simultaneously) and the requirements of special instrumentation (such that the tools are not influenced by the strong magnetic field or introduce artifacts in the images) make it possible to acquire intraoperative images at any time throughout the surgical procedure without moving the patient. The images themselves are obviously inferior to those obtained by a full-scale 1.5 – 2.0T MR scanner, but still possess enough spatial and temporal resolution for their intended purpose (differentiate soft tissue types, assess anatomy and monitor a surgical procedure for resection extent and hemorrhaging) [8]. There are several disadvantages of this method of intraoperative feedback. The area between the magnets is sufficient but nonetheless a limiting factor for the movements of medical personnel and the selection of instrumentation to co-exist inside an MR scanner was described in [8] as "...[a series of] persistent and occasionally painstaking trials..." and cited lack of availability of MR-compatible instruments for hindering the implementation of the MR suite. The cost involved in carrying out such a project is certainly prohibitive for many centers although such a facility does provide valuable information.

The route taken by another group of researchers in [7] was to provide intraoperative MRI capabilities whilst locating the MR scanner in an adjacent room. This

environment has been dubbed a 'twin operating theater' and is similar to that used for intraoperative CT. The group in [7] use a Siemens MAGNETOM OPEN (0.2T field strength) MR scanner and move the patient from a full operating theatre to the scanner when necessary to acquire intraoperative data sets. This system has the advantages of not requiring 'MR-compatible' instrumentation (thereby reducing costs) but has the disadvantages of requiring an interruption in the surgical procedure to physically move the patient from the OR suite to the scanner room.

A far less costly and less intrusive alternative to the aforementioned intraoperative CT and MRI imaging is intraoperative ultrasound. Although traditional ultrasound B-mode (tomographic) images are inferior in image quality and spatial resolution (versus CT and MRI images), they are still capable of providing relevant information during biopsy, cyst aspiration and tumour resection. More recently, 3D ultrasound imaging as well as doppler ultrasound has enabled the acquisition of intraoperative volumes of interest and blood flow velocity information during the course of the surgery.

1.4.2 Functional

Functional information that is used during the surgical procedure is primarily limited to the imaging studies (PET, fMRI, cortical electrode mapping) performed preoperatively. During the procedure, the surgeon may obtain a more accurate assessment of the margins of critical areas through the use of a stimulator. In this way, the surgeon is able to identify functional areas from the responses of a still conscious patient about the sensations that he/she may perceive.

1.4.3 Vasculature/Blood Flow

Acquisition of cerebrovascular images in the intraoperative setting can be accomplished through the use intraoperative digital subtraction angiography (DSA), intraoperative magnetic resonance angiography (MRA), and doppler ultrasound (US). Intraoperative vasculature imaging can be important to assess the result of surgery to correct arterio-venous malformations (AVMs) and as surveillance against hemorrhage. Intraoperative DSA and intraoperative MRA images can be taken (with the appropriate

specialized equipment) at various points through the surgical procedure to assess the vasculature and doppler US can be used to measure cerebral blood flow velocities.

1.4.4 Conclusion

In this section, several alternatives for providing intraoperative feedback have been described. Although these methods do indeed furnish useful data which the surgeon can use, they do so at the expense of incurring substantial financial cost, specialized equipment and prolonging and/or altering the surgical procedure itself. The project described in this thesis provides a trade-off in contrast with the other methods discussed in this section: to provide intraoperative feedback to the surgeon while using an existing IGNS environment and therefore not incurring any substantial costs. While the updating provided in this project is in no way comparable to an intraoperative MRI scan, it does still provide feedback on the current state of tumour resection overlaid onto preoperative data.

In addition to the imaging methods discussed above, efforts are underway for providing the surgeon a view of the current state of the patient's anatomy through more novel means. Two such efforts are underway in our laboratory. The first method uses intraoperatively acquired ultrasound data to update preoperative acquired volumetric data that the surgeon is using for intraoperative visualization and guidance [2]. A second approach uses cortical surface information acquired with a laser rangefinder to detect and then propagate intraoperative changes to the preoperative volumetric data upon which the surgeon so heavily relies [3].

1.5 Relevance of Intraoperative Feedback

The intraoperative acquisition of data through the means discussed above and through this project address many important inadequacies in the current state of IGNS using preoperative information only. The following sections describe the benefits of intraoperative feedback in both the intraoperative as well as the postoperative settings.

1.5.1 Intraoperative Aspects

The acquisition of additional data using sophisticated equipment such as intraoperative CT and MR suites has the advantage of providing the surgeon with the current state of the patient's anatomy and checking for the extent of tumour resected and for any hemorrhaging that may have occurred during the course of the operation. These methods of intraoperative feedback provide extremely useful information to the surgeon at the expense of prolonging the procedure to varying degrees, altering the work of the surgeon and requiring expensive specialized equipment and instrumentation. The prohibitive expense of this equipment limits its use to a select few centers worldwide. It is obvious that intraoperative feedback of some sort would be of great benefit to the vast majority of centers without such equipment who also perform neurosurgical procedures in order to facilitate improved visualization and outcomes for the patient. It is with this fact in mind that this project and other projects developed in our laboratory [2,3] are intended.

1.5.2 Postoperative Aspects

The gathering of intraoperative data furnishes useful information for the postoperative setting as well. Firstly, the use of intraoperative data can be used to verify that a pathology is fully resected and that there is no hemorrhaging prior to closing the skull and terminating the surgical procedure. After the procedure has been concluded, the data collected during the procedure can be examined postoperatively along with follow-up scans and subsequent neurological examinations and testing to gauge the overall success of the surgical intervention. Information provided by the intraoperative can also be useful to the neuropsychologist in studies of the correlation of the degree of resection of various areas with preoperative and postoperative neuropsychological testing and any associated postoperative psychological manifestations.

1.6 Thesis Objectives

The preceding sections have briefly presented the current state of an IGNS environment and its primary elements. Its shortcomings have been presented and the

relevance of intraoperative feedback to address these shortcomings has been detailed. Therefore the motivation for this project is clear.

The purpose of the project described in this thesis is to provide intraoperative feedback to the neurosurgeon using the equipment comprising a typical IGNS environment. The project accomplishes this task through the use of physically based deformable models. The major objectives for this mode of intraoperative feedback are:

- to provide useful visual and quantitative feedback to the neurosurgeon about the progress of tissue resection during a surgical procedure
- to provide this information using the equipment available in a typical IGNS environment, without the use of any specialized and possibly prohibitively expensive additional equipment such as an ultrasound machine, open coil MRI, etc.
- to provide this feedback while simultaneously being unobtrusive to the surgeon's work

The organization of this thesis is as follows. An overview of historical developments in neurosurgery, as well as a discussion of medical imaging techniques, positioning device technologies and the issue of accuracy of IGNS is presented in Chapter 2. The mathematical development of the deformable model used in this project, description of algorithm used and calculation of the volume estimation quantitatively determining the extent of resection is detailed in Chapter 3. Chapter 4 discusses the implementation of the deformable model in computer software within the context of VIPER, the use of the FARO Surgicom for data acquisition and real time interactivity issues. The validation of the deformable model's capabilities through experimental trials in detailed in Chapter 5. Chapter 6 gives an overview of how the intraoperative feedback developed in this project is integrated into the IGNS environment in the OR. Finally Chapter 7 draws conclusions from the work presented in this thesis and provides further extensions of this work in conjunction with ongoing work in our laboratory.

Chapter 2

Image Guided Neurosurgery (IGNS)

2.1 Historical Overview of Developments in Neurosurgical Guidance

Due to the specific demands of performing surgery on the brain such as the very delicate nature of the tissue, the ability to open the skull and the existence of areas of vital brain function and vasculature throughout the brain, the surgeon cannot perform extensive exploration or manipulate the brain tissue to a large degree. The objective of the surgeon is to make the minimum opening to the skull that will guarantee access to the entire surgical site of interest whilst respecting the functional importance and the oxygen carrying vasculature of the tissue lying between the surface of the brain and targeted site [9]. The surgeon must also contend with the facts that pathological tissue is not always visually distinguishable from normal tissue and that procedures targeting deep-seated lesions do not permit direct visualization. These considerations have led to techniques for planning and precisely localizing the pathology and areas of vasculature and vital brain function prior to the surgical procedure. This section examines the major developments in stereotaxic (or stereotactic) neurosurgery during the last century.

2.1.1 Frame Stereotaxy

The terms *stereotaxic* and *stereotactic* are often used in connection with neurosurgery to denote a surgical technique utilizing some sort of surgical guidance. The terms themselves are from the Greek 'stereo', meaning three-dimensional, the Greek 'taxis' meaning 'arrangement' and the Latin 'tactic' meaning 'to touch'. The two terms are often used interchangeably; in this document the terms 'stereotaxy' and 'stereotactic system' will be used to reference the same techniques for surgical guidance. *Frame stereotaxy* can be formerly defined as the technique for locating targets of surgical interest within the brain relative to an external frame of reference [9].

Perhaps the first documented case of the use of a mechanical frame fixed to anatomical landmarks is that of Horsley and Clarke in 1908 [10]. They used a primitive frame to allow placement of electrodes within an animal brain to establish a positional brain atlas. This was significant since it showed that target points within the brain could be reproducibly localized using a frame for electrode placement. In 1947 Spiegel and Wycis published a paper describing a device for human stereotaxy. Their frame used landmarks within the brain from pneumoencephalograms as reference points. Frame stereotaxic procedures grew into the 1960's, declined due to the introduction of therapeutic agents such as L-dopa and then re-emerged with the development of CT [9].

The technique of frame stereotaxy involves the attachment of a rigid frame (an example of which is depicted in *Figure 2.1*) to the skull by means of pins or screws. The frame itself is put in place on the patient prior to imaging and is scanned along with the patient's head. The frame itself, when imaged with CT or MRI, provides landmarks external to the skull on the periphery which can be used for registration purposes. Attachments to the frame allow for surgical tools to be attached for biopsies and aspirations. Precision guides are used to set an accurate trajectory into the brain to the site of surgical interest. Since a frame is in place on the patient during the surgical procedure, it is primarily used for electrode placement, biopsy of suspect tissue and for aspiration of cysts. If a large opening must be made to the skull, in the case of a craniotomy for example, the frame can represent a significant constraint to the surgical field. It is for these situations that so-called *frameless stereotactic systems* were developed.

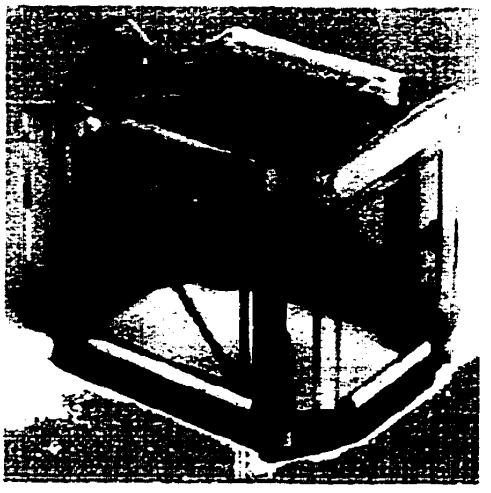

Figure 2.1 The Olivier-Bertrand-Tipal (OBT) stereotactic frame.

2.1.2 Frameless Stereotaxy

A *frameless stereotactic system* is a system which strives to achieve accuracy comparable to a frame-based system without the use of a frame. Such systems rely on an accurate localizing device and registration or correspondence of points from the surgical or patient space to the image space. The use of a frameless stereotactic system facilitates a wider range of surgical options when a craniotomy must be performed by virtue of the fact that there is no frame present on the patient's head and its surface is free from obstruction (aside from the Mayfield clamp which must be used to immobilize the patient's head) facilitating minimal interference with the surgical procedure. A typical frameless stereotactic system consists of a position tracking device (discussed in detail in Section 2.3) rigidly fixed to the operating table or Mayfield clamp (which in turn rigidly fixes the patient's head) and a computer display of preoperative images from various imaging modalities (discussed in the following section). An affine transformation (system is assumed linear) is used to relate the position of the tracking device, often in the form of a probe, to the preoperative images displayed on the computer display. The surgeon manipulates the probe and uses its position with respect to the patient and corresponding position in the display of images to ascertain his/her position for trajectory planning and in the approach to the site of interest. The preoperatively acquired data sets allow accurate (to within a few millimetres [11]) interactive localization of surgical target locations and

trajectories [12]. It is to this type of system that the project described in this document has been applied.

2.2 Imaging Modalities

The wealth of imaging modalities currently available to the neurosurgeon have the potential of providing extensive patient information on all aspects, from anatomical to functional and vasculature information. The surgeon makes use of as many imaging studies as deemed necessary in order to obtain the 'complete picture' of the surgical case and uses the information to plan a successful procedure. This section examines the primary imaging modalities used for examining the patient and their place within the typical IGNS environment.

2.2.1 Anatomical

The anatomical information afforded by the two primary neuroimaging technologies, computer assisted tomography (CT) and magnetic resonance imaging (MRI), provide the 'backdrop' or the primary context upon which the IGNS environment is built. CT images are produced using several thousand measurements of x-ray transmission to analyze a plane in the body. These planes, or tomographic slices, are built up into a data set that is reconstructed to form a 3D view of internal structures within the cranium. The development of CT in the 1970's brought about a resurgence in the use of stereotactic procedures and recently fast CT imaging techniques such as spiral CT [13] have enabled intraoperative imaging studies to be performed (see *Figure 2.2*). CT is excellent for rendering the geometric accuracy of structures that are easily visualized with x-rays, such as bones and air cavities and has good spatial resolution (1-3mm) [13]. Disadvantages of CT include exposing the patient to radiation and poor differentiation of soft tissue types relative to MRI, although contrast in the images can be improved through injection/ingestion of x-ray absorbing materials [13].

Figure 2.2 A spiral CT scanner in intraoperative use.

MRI is a more recent imaging technique made by the selective detection of proton resonance decays in the body after alignment (by a large static magnetic field) and perturbation (by RF pulses). The spatial position in the body is determined by modifying the resonant proton frequency through application of spatially varying magnetic fields and by observation of the resulting changes in spin phase [13]. Use of different pulse sequences and other techniques such as the introduction of contrast agents such as gadolinium enable excellent differentiation of soft tissue types with high spatial resolution (~1 mm). MRI is subject to imaging non-linearities [11], artifacts caused by patient motion during longer scan times and the expense and large space requirements for the equipment. Innovative designs using smaller and different coil geometries have facilitated the introduction of MRI into the OR suite for intraoperative imaging [14]. Two examples of intraoperative MR scanners are shown in *Figure 2.3*.

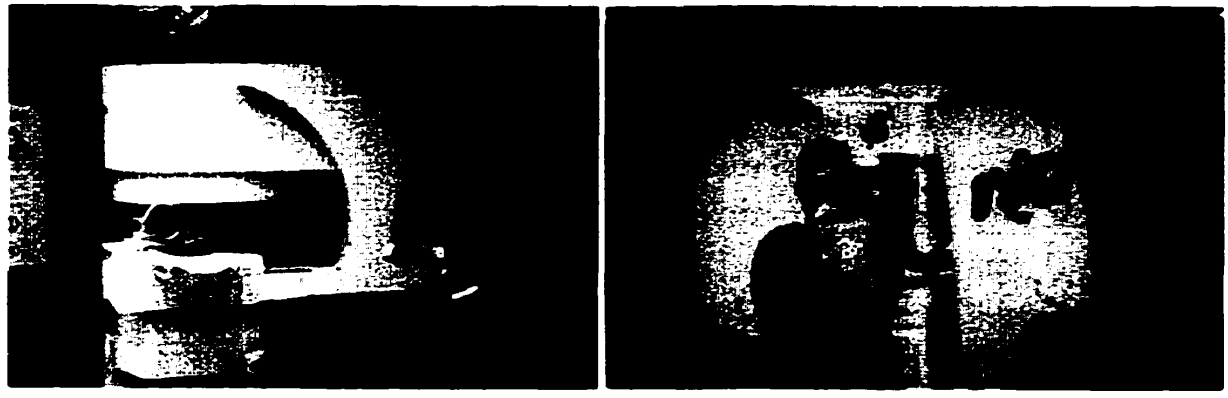

Figure 2.3 Different configurations of intraoperative MR scanners.

Ultrasound (US) imaging, although inferior to MRI and CT in image quality and spatial resolution (~5mm), nonetheless finds utility as a viable neuroimaging modality for providing biopsy and aspiration needle guidance and for viewing progress in tissue resection. US images are formed by propagating ultrasonic energy into the body by means of a transducer which acts as a transmitter of the incident signal and a receiver of the reflected signal. The time delay between the incident and reflected signals is a function of the acoustic impedance of the tissue traversed and is used to obtain depth information to create a cross-sectional 2D image. Three dimensional US images can be built up from a series of 2D images with detector arrays and/or mechanical motion of the transducer. The speed of US imaging, along with the lower equipment cost and OR space occupied make US an attractive option for intraoperative guidance. US imaging is subject to shadowing artifacts, specular noise and lower spatial resolution. In addition, there are limits in the ability to place and move the ultrasound transducer on the surgical field, making it difficult to image deep-seated lesions and resections in some instances and spatial resolution not sufficient for lesions smaller than 5mm or to clearly define and guide the total resection of tumor margins [14].

2.2.2 Functional

Non-invasive cerebral mapping techniques have evolved to localize functionally important cortical areas. They attempt to resolve the spatial and temporal distribution of neuronal activity during behavioral and cognitive tasks by measuring one of two

physiologic responses: electromagnetic response or hemodynamic/metabolic response. Magneto-encephalography (MEG) and electroencephalography (EEG) measure electromagnetic response and positron emission tomography (PET) and functional MRI (fMRI) measure the hemodynamic/metabolic response. These modalities are typically correlated with MRI and/or CT using some type of image co-registration and fusion algorithm to provide anatomical context [15]. The purpose this functional imaging is to provide an insight into brain activity so that areas of vital brain function may be spared during a surgical intervention.

One of the most frequently used functional imaging modalities, positron emission tomography (PET) imaging is used to visualize areas of high metabolic activity while the patient is carrying out a specific task such as listening to tones, performing a mental calculation, viewing a light or performing a motor function. The PET scanner is sensitive to a radioactive tracer substance (which is harmless to the patient) which is given along with a brain nutrient such as glucose. The tracer serves as a visible marker in the PET image; attached to the invisible (in the PET image) nutrient it allows the observer to follow the progress of the nutrient through the brain in order to locate areas where the nutrient is preferentially metabolized for energy while the patient carries out a task. Those areas which exhibit high metabolic activity during the performance of a task are then associated with that task. To form the PET image, the tracer emits positrons that collide with electrons to produce gamma ray emissions which the scanner registers. The intensity of the photons is a function of the degree of chemical activity in a particular region. An example of a typical PET image is shown in *Figure 2.4*.

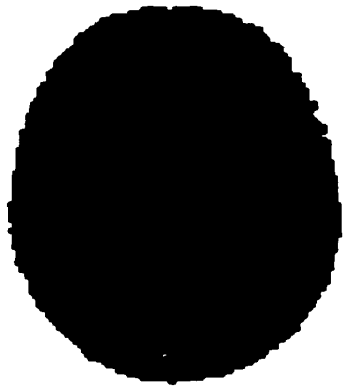

Figure 2.4 A typical PET image, showing regions of increased metabolic activity.

Functional MRI (fMRI) can combine detailed anatomical information with precise physiological information to create a structural and functional model of an individual's brain. This imaging technique uses a measure of the ratio of deoxygenated to oxygenated hemoglobin to obtain a measure of blood flow to different regions of the brain. This information can be used preoperatively for surgical planning and intraoperatively for guiding surgical resection strategies. The combination of anatomical and physiological information makes fMRI an excellent tool for intracranial navigation [15]. Examples of typical fMRI images are shown in *Figure 2.5*.

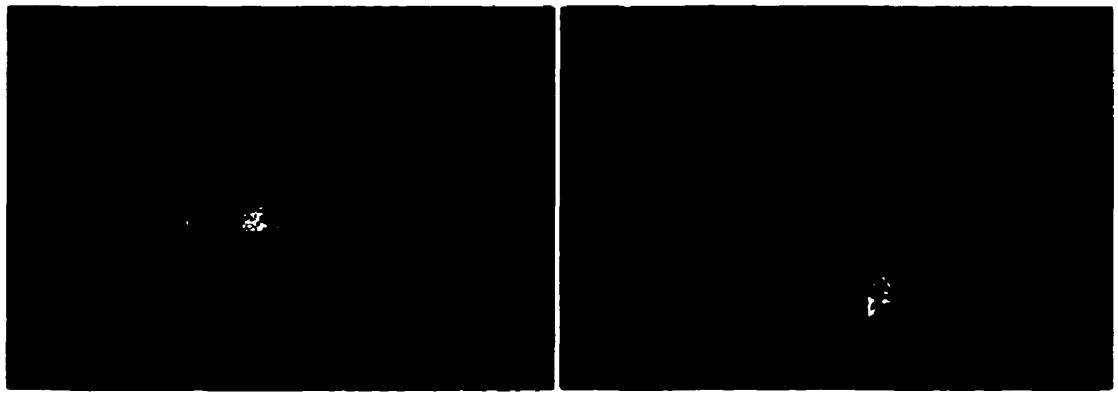

Figure 2.5 Examples of fMRI images. Information from fMRI imaging is shown in a cross-sectional image at left and in a 3D reconstruction at right.

Measurement of the electromagnetic response of the brain is also an important technique in the determination of functionally important regions. EEG recordings made

preoperatively with an array of electrodes affixed to the head as well as monitoring of depth electrode signals serve to pinpoint foci of epileptic centres and other electroencephalographic abnormalities. The recorded EEG potentials may then be labelled as markers superimposed on the preoperative images or interpolated to produce a surface mapping of EEG activity [16]. Intraoperatively, the surgeon may stimulate brain regions while the patient is conscious in order to delineate vital speech, sensory and motor areas.

2.2.3 Vasculature

The focus of vasculature imaging is to supplement anatomical information in order to approach intracerebral locations safely without puncturing blood vessels. This is critical during implantation of depth electrodes and in resection of tumours. The following section describes some vasculature imaging modalities.

Digital subtraction angiography (DSA) images are x-ray angiograms that are taken stereoscopically. For example, at the MNI a C-arm DSA system is used to perform the angiographic acquisition twice at gantry angulations separated by approximately 7 degrees (which corresponds to the vergence of the eyes for binocular viewing) [17]. A special fiducial marker system and calculations performed on a PC-based system permit a correspondence between points in the stereoscopic images and points in the 3D MRI and CT volumes. The position of the tracking device used in the frameless stereotactic system is coupled to the stereoscopic DSA display so that trajectories to surgical sites of interest can be planned whilst respecting the cerebral vasculature present. Accuracies of stereoscopic DSA approach 1mm using both AP and lateral DSA images. Although the presentation of cerebral vasculature via stereoscopic DSA allows the surgeon to perceive the 3D relationships of vessels and is of tremendous advantage over standard planar angiograms, the technology is not inherently 3D. Also, DSA imaging requires subjecting the patient to ionizing radiation, which is sometimes undesirable. The introduction of magnetic resonance angiography (MRA), an inherently 3D imaging modality which is safe for the patient, has to an extent supplanted DSA in the visualization of cerebral vasculature.

MRA is an imaging technique for the visualization of the cerebral vasculature using the MR scanner. Indeed, it is often performed during the session in which the anatomical scans are acquired. The technique produces images of flowing blood, the intensity of the images being proportional to the velocity of the flow. MRA has lower spatial resolution and accuracy relative to stereoscopic DSA, but possesses the advantages of being a 3D modality – namely that the 3D cerebral vasculature can be viewed from any arbitrary viewpoint. This factor alone is useful in removing ambiguities in the images and permits greater flexibility for the neurosurgeons when visualizing intracranial trajectories [18]. MRA images can be constructed from the raw 3D volumetric data set through one of two methods. A surface-rendered version of the cerebral vasculature tree can be constructed using manual and semi-automatic segmentation, but this method is labour and time intensive and can result in discontinuities in the representation. Volume rendering of the MRA data set using a technique call *maximum intensity projection* (MIP) is a faster method relative to surface rendering of the data, since the time-consuming segmentation step is bypassed [18]. Variants of the MRA technique, including time-of-flight (TOF) angiography and phase contrast angiography as well the use of contrast agents such as gadolinium have been developed to provide further image contrast and quality. Examples of MRA images are shown in *Figure 2.6*.

Figure 2.6 Some examples of typical MRA images.

As was the case for ultrasound anatomical imaging, Doppler ultrasound is a safe and reliable technology for measuring cerebrovascular blood velocities. Ultrasonic energy

at frequencies of approximately 2 MHz is directed at vascular formations within the skull by a handheld transducer. The frequency or *doppler shift* in the reflected sound is proportional to the velocity of the reflecting matter (the blood). Using intracranial ultrasound, one can observe velocities from the cerebral arteries, the internal carotids and the basilar and vertebral arteries by varying the transducer location, angle and depth setting (focal length) [19]. The visual display of doppler ultrasound consists of a traditional B-mode ultrasound image (ie. cross-section) with color-mapped regions to indicate the direction of blood flow and the magnitude of the flow velocity. An example of a Doppler ultrasound image is shown in *Figure 2.7.*

Figure 2.7 Doppler ultrasound image of the heart.

2.3 Frameless Stereotactic Neurosurgery using Computer Display and Position Tracking Devices

The typical IGNS environment utilizing a frameless stereotactic system is comprised of a position tracking and a computer display of images from various imaging modalities. This section describes the information that is presented to the surgeon in the computer display and the various types of position tracking device technologies that are currently available.

The computer display of preoperative images (and possibly intraoperative images as well) upon which the surgeon relies for planning and guidance in a frameless stereotactic environment has the capability of providing a vast array of information about the patient. It is vital that the information is rendered in a clear fashion with an intuitive

interface which allows for rapid retrieval of additional data and varying of parameters such as zoom and translucency of the surface representations for example. The images displayed include standard triplanar views (axial, sagittal and coronal) of anatomical information, usually from MRI or CT. The position of a localizing device is superimposed on the triplanar view to allow the surgeon to correlate his/her position on the patient and in the images simultaneously. The position of the probe may be illustrated in the images as crosshairs in the 2D images or as a rod representation in a 3D display. Trajectory views depicting a plane perpendicular to the probe are possible allowing evaluation of structures traversed during a biopsy or cyst aspiration for example. Often, functional images (PET, fMRI, EEG data) are overlaid on the anatomical images to relate the proximity of the surgical site of interest to regions of vital brain function. Vascular information (DSA, MRA) may also be incorporated, either overlaid in the display or on a separate display. Three dimensional representations, such as surface renderings of objects segmented from MRI data, can also be displayed to give the surgeon a better sense of relationships between structures than is provided in the 2D images. Some examples of different IGNS displays are shown in *Figure 2.8* and *Figure 2.9*. *Figure 2.8* depicts a typical screen of information from VIPER showing the standard 2D tri-planar views and a 3D view at lower left. *Figure 2.9* shows a screen of MedViewer, allowing for multiple windows of information to be displayed, as well as overlaying of multiple modalities.

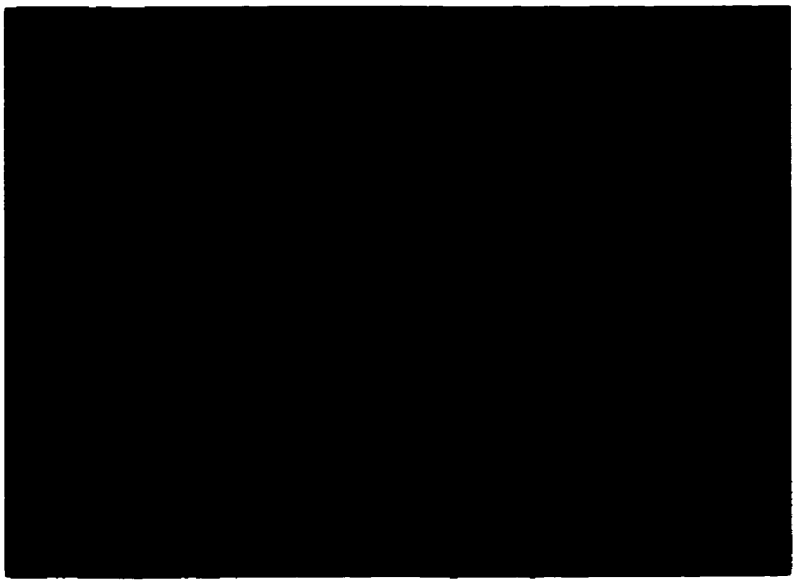

Figure 2.8 Image from VIPER IGNS software.

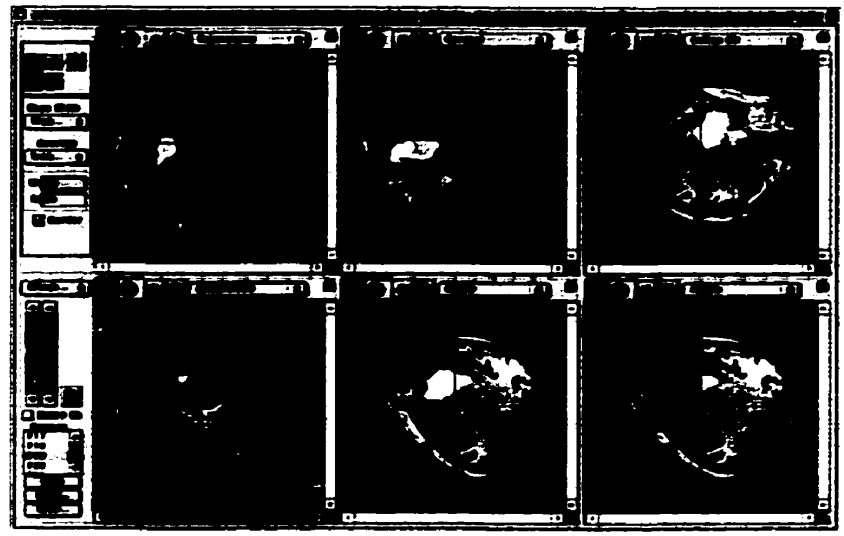

Figure 2.9 Image from MedViewer IGNS software

The position tracking device in an IGNS system provides the correspondence between the physical location of a probe with respect to the patient and its position relative to the preoperative images used for guidance. Several different technologies have been developed to implement position tracking devices and some of these are more appropriate for neurosurgical applications. The position tracking device used at the MNI and at several other centers is an articulated arm, such as the FARO Surgicom (FARO Industries, Orlando, Fla) [20] shown in *Figure 2.10*. The passive arm uses digitized voltages derived from precision potentiometers in each of the joints to determine their angles and, through a series of transformations, the position of the probe relative to its base. Articulated arms provide a number of advantages in a frameless stereotactic IGNS system over conventional frame and instrument holders, including providing minimal interference with the surgical field since they can be moved out of the way when not in use and providing great flexibility of the choice surgical trajectory. The use of the FARO Surgicom in this project will be detailed in Section 4.4. Optical position tracking devices [21-23] track the position of LEDs or illuminated markers with several cameras using a triangulation technique [24,25]. These systems require a clear line of sight which can be difficult to achieve in the OR. Ultrasonic systems [26] using time delays between incident and reflected sound are subject to accuracy degradation by air temperature and echoes in the OR. Magnetic

systems [27] determine location using magnetic field gradients but ferrous materials from instruments and equipment in the OR as well as electromagnetic inference can degrade their accuracy.

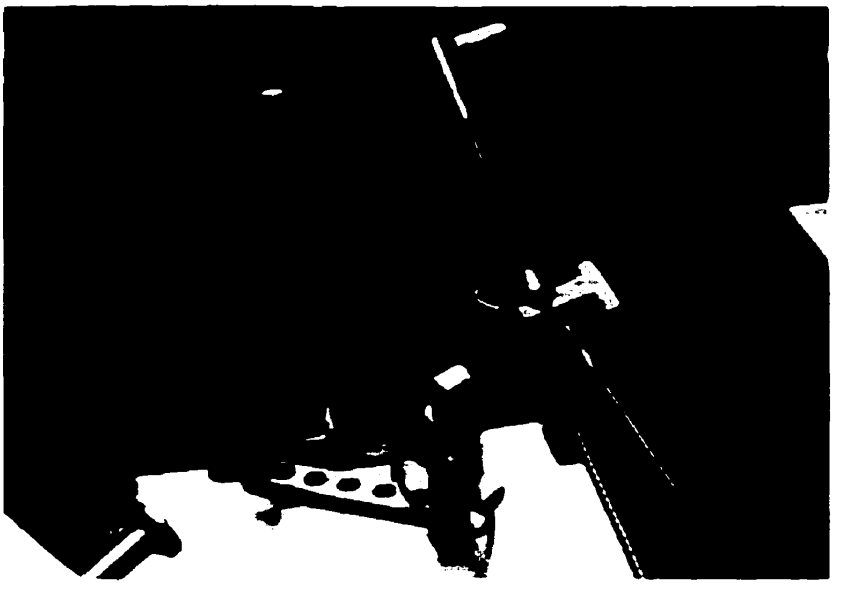

Figure 2.10 The FARO Surgicom articulated arm position tracking system.

2.4 The Issue of Accuracy in IGNS

There are several sources of error that can degrade the accuracy of a frameless stereotactic IGNS system [28]:

- resolution of the preoperative images
- image artifacts (patient motion during acquisition, geometric distortions)
- accuracy of the position tracking device used for guidance
- accuracy of the registration between the preoperative images and the position tracking device
- change in the position of the brain between the time of imaging and surgery or changes in the brain during the surgical procedure

This section will briefly discuss registration error and intraoperative brain movement as sources of error in such a system.

2.4.1 Registration Error

Registration allows the determination of the linear relationship between two coordinate systems [11]. This mathematical process allows the location data acquired with the position tracking device with the respect to the patient to be transformed to the coordinate system of the images displayed on the computer screen. Measurement errors from the accuracy of the position tracking devices, the human error introduced when acquiring data points with the probe and selecting the homologous points in the images and the assumption of linearity serve to degrade the accuracy of the registration process. A detailed examination of registration error can be found in [11].

In frame-based systems, fiducial markers on the frame itself are used for the registration process. These points are clearly visible in MRI and CT images and as well as being accurately defined on the frame. Since the frame markers are rigid there is absolute stability between the location of these fiducial points between imaging and surgery.

For frameless stereotactic IGNS systems, the fiducial markers must lie directly on the patient. Extrinsic fiducial markers screwed into the outer table of the skull may be used to provide rigid points, or markers may be glued to the skin prior to imaging but these are subject to the movement of the skin when surgical incisions are made or due to the effects of gravity. Intrinsic fiducial markers, such as the tip of nose, nasion, tragus or locations on the orbital rims, may be suitable as points of commonality in the scan as well as on the patient. It can be difficult to find these types of intrinsic points, however, since they must be clearly visible on the CT or MRI, have rigid attachment to the head and have well defined shapes for exact point location for accurate registration.

There are several different methods used for registration. Homologous point matching (HPM) [29] is a technique whereby a set of data points is sampled on the head of the patient using a position tracking device and the corresponding points are then identified in the preoperatively acquired MRI or CT data set. An affine transformation matrix is computed by calculating the least squares distance between the two sets of points. Surface matching [29] is another technique whereby a set of data points is sampled on the surface of the patient using a position tracking device and a surface match (least squares sense) is performed between these points and a 3D surface computed from a MRI

or CT data set. This is an iterative process and can be considered a supplement the HPM method [29].

Although the frame-based registration techniques are likely the most accurate due to their rigidity and well-defined shapes, there are many situations where the use of a frame is not feasible. A tradeoff is therefore made to use frameless stereotactic techniques which are somewhat less accurate but allow greater freedom for the surgeon. A good discussion of registration accuracy is presented in [11].

2.4.2 Intraoperative Brain Movement

A subject that is not addressed by most current IGNS systems is the change in brain position that occurs throughout the surgical procedure. The accuracy of the preoperative images used for surgical guidance are progressively degraded as this movement occurs. The intraoperative imaging techniques discussed in Chapter 1 are an attempt to intraoperatively acquire new data during the procedure to reflect the current state of the surgical intervention. Other novel methods for intraoperatively updating preoperative images were also described. The project described in this document is not aimed at updating the current state of the preoperative images; rather the intent is to supplement these images with tissue resection progress to provide the surgeon with useful intraoperative feedback while still using a typical IGNS environment.

The position of the brain can change relative to the preoperative state in which it was originally imaged for a variety of reasons [28]. When the skull and dura are opened, changes in intracranial pressure can exert an alteration in the position of the brain, as can the effect of gravity and loss of support from the skull itself [30]. Throughout the surgical procedure, changes in blood and cerebral spinal fluid (CSF) pressure, the introduction of osmotically active drugs such as mannitol which alter the brain's water content and the removal of tissue during a resection can all alter the brain's position and therefore degrade the accuracy of the preoperative images that are used for guidance. Research reported in [11] found that the brain most often sinks relative to its preoperative position. This finding has a direct effect on the accuracy with which the surgeon can judge his/her depth into the brain in the vicinity of the brain's surface. Due to the intraoperative brain

movements discussed above, the research in [11] surmises that no frameless stereotactic IGNS system could be more accurate than 3mm.

Chapter 3

Use of Deformable Models for Intraoperative Feedback

3.1 Introduction

This chapter provides a full elucidation of the mathematical details of the deformable model used in this project. Implementation details are reserved until Chapter 4. The rationale for the choice of deformable models over other alternatives is discussed. The variables used in governing the behavior of the deformable model are described and the method used for computation of a volume estimate of the resected cavity is presented.

3.2 What are Deformable Models?

Deformable models are derived from an active area of interdisciplinary research termed physically based modelling. Physically based modelling deals with the realistic modelling of objects by simulating the elastic properties of real world objects that influence and constrain their motion and dynamics. This area combines elements of geometry, physics (elasticity theory) and approximation theory (solution by finite element analysis and numerical integration). The applications of this modelling technique range from realistic computer graphics rendering for film to medical imaging segmentation and surgical simulation.

There are several excellent surveys in the literature discussing the use of deformable models in medical image analysis[31, 32]. Seminal work by Terzopoulos from 1986 to the present has first described and then expanded the notion of deformable models from a new computer graphics construct to a robust method for surface fitting and medical image segmentation, incorporating methods for dealing with topological changes (ie. segmenting vasculature from MR data that is discontinuous). The work presented here is a new application of Terzopoulos' work: an extension to real time intraoperative applications.

3.3 Why Use Deformable Models?

The search for a solution to the problem of providing intraoperative feedback in the OR using an existing IGNS system necessitated a thorough examination of current mathematical and computer graphic methods for producing an accurate representation of the degree of tissue resection subject to the specific constraints involved in this problem. A successful solution would necessarily involve a model capable of producing a surface from a sparse number of irregularly spaced data points and would require little or no user interaction to control the model's behavior. During a resection procedure the surgeon must only acquire data points as he/she performs the resection; there should be no need for a technician to adjust parameters to govern the behavior of the model in accurately representing the resection cavity.

A review of the literature produced a number of methods with potential applicability to the problem. These methods can be grouped into four areas:

- curve/surface fitting
- non-uniform rational B-spline (NURBs) methods
- physically based modelling (snakes, balloons, active surfaces)
- other methods, such as solid modelling and level set methods

The following discussion briefly outlines each of the methods investigated and the rationale for the selection of the use of deformable models in this project.

An investigation into curve and surface fitting methods was initially undertaken as a solution to the representation of resection cavities. Curve and surface fitting involves finding the 'best' fit of a set of data points to a curve or surface. The conditions of optimality for fitting a curve or a surface to a set of data points can be the mean square distance between the points and the curve or surface. These methods often utilize different families of polynomials such as Bezier and Hermite, which possess different properties and control point types which govern their behavior [33]. This method tends to be more applicable to regularly spaced data points and dense data (such as from a rangefinder for example) than the sparse irregularly spaced and clustered data encountered in the problem at hand. Experiments were undertaken with the fitting of B-splines to acquired data and

the results were found to be unsatisfactory. The third order curves did not adequately represent sharp corners and the use of the curves created a tendency to acquire the points in a specific topology (ie. acquiring the points in a series of 'ribs' lining the resection cavity). The use of surface patches (piecing together of multiple sections to form a representation) would likely be required to accurately represent a resection cavity, and this would be difficult to achieve with little or no user interaction.

An extension of curve and surface fitting is a general class of methods utilizing non-uniform rational B-splines (NURBs). Again, a surface can be constructed from a series of lines or through the use of surface patches and the degree of the polynomial basis function used is an important factor in their behavior in adapting to a given set of data points. For example, an adequate representation of a sharp corner would require a higher order polynomial relative to the representation of a smooth surface. These curves also utilize control points to govern their behavior; the manipulation that the control points afford can be of great utility to a graphic designer but they are less desirable in this project due to the importance of having minimal user involvement in the rendering process. More recently, a form of NURBs, known as dynamic NURBs[34], has been presented in the literature. These methods integrate equations of motion and material properties through the use of finite element modelling to provide a more intuitive interface for the graphic designer. The incorporation of physically-based modelling into the NURBs formulation made this method attractive for application in the project, but control points are still retained and the method is not amenable to the fitting of the topology of the data encountered in this project.

Some of the other methods investigated for this project included solid modelling, free form surfaces and level set methods. Solid modelling [33] involves the use of geometric primitives to model manufactured parts and other somewhat regularly shaped objects. These methods were quickly dismissed due to their inability to model complex shapes and conform to a set of data points of arbitrary topology. These were important in that they fostered the idea of a parameterized surface, which ultimately led the author to investigate superquadrics and ultimately influenced the choice of physically based modelling for this project. Level set methods, as described in the work of Sethian [35-37], were investigated

early in the project. These methods are very flexible, can be applied to arbitrarily complex shapes and can operate on both 2D and 3D data to segment data using a formulation of a Hamilton-Jacobi type equation to propagate a 'front' through the data. The front is described in [35] as a "... closed, non-intersecting hypersurface flowing along its gradient field...". The front uses gradient information within the data to stop in the vicinity of object boundaries. The application of level set methods to medical image segmentation applications is obvious and their ability to change topology gives them particular applicability to the segmentation of vasculature. Early in the stages of the project, thought was given to implementing this method if intraoperative ultrasound would be used for data acquisition. Although not amenable to data acquisition with the FARO Surgicom (data too sparse), the combination of level set methods and 3D ultrasound data remains a viable alternative for intraoperative visualization of tissue resection.

Physically-based modelling, involving a parameterized surface and finite element modelling to produce global and local deformations respectively, was thoroughly investigated and ultimately chosen for application in the project. Although several authors, namely Pentland et. al. [38-43] and the Cohens [44,45], have made extensive contributions to the literature in the areas of active contours and balloons (Cohens), and physically based models with deformation modes (Pentland), it remains the work of Terzopoulos that has developed physically based or deformable models to a large degree. Deformable models incorporate equations of motion and use finite element techniques to effect the deformations they achieve. Physically-based, or deformable models are amenable to the application of modelling cerebral tissue resection in that they possess the following characteristics:

- they have the ability to assume complex freeform shapes (which is a requirement in modelling tissue resection)
- they can interpret the sparse data available as applied forces to the deformable model; thus a visualization can be achieve with relatively few data points
- behavior is predictable, intuitive and controllable with few parameters
- can be parametrically defined as an open surface such as a plane (used in the project), or a closed surface such as a sphere or superquadric

- superior to simpler (albeit less computationally intensive) spline based sculpting approaches due to the greater predictability and lower degrees of freedom involved since there can be no means for user interaction on how the data points are applied to achieve the desired deformation

In addition to the applicability of deformable models in this project, they are finding application in other areas of medical imaging such as in the segmentation of boundaries and surfaces from image and volume data, where gradient info is used to provide image forces to deform the model.

Although the deformable models used in the project utilize 2D finite elements in their formulation, the technique can be extended to the use of 3D finite elements. Several researchers have developed 3D finite element models to model tissue deformation during surgery [46,3] and for the purposes of surgical simulation [47-50], where forces on the virtual model are derived from sensors attached to physical instruments that resident surgeons can use for developing their surgical technique. Due to the greater computational expense incurred with the use of 3D finite elements, methods focusing on reducing the computational load are often focused on.

3.4 Mathematical Development of the Deformable Model

The mathematical development of the deformable model used for intraoperative feedback is presented in the following paragraphs. The mathematics of the model are presented first, followed by their solution via finite element techniques.

Mathematics of the Planar Deformable Model

The deformable model used to provide intraoperative visualization is an open, planar rectangular surface representing a scalar function $z(x,y)$, similar to that described in [51]. The scalar value of z represents the lateral displacement of the surface away from its original planar shape. The surface is discretized into 2D rectangular finite elements with Hermitian interpolation functions. These elements are formulated as a thin plates under tension to model a material with elastic properties. The deformable model is envisaged as

an elastic sheet made of a suitable material such as rubber. Parameters in the model allow for adjustment of the surface material's properties, such as its global rigidity and its susceptibility to local deformation when forces are applied. In order to encompass the above properties, the deformable model is formulated as a problem in variational calculus, expressing the deformation of the surface in terms of an energy functional.

The total energy of the deformable surface model is represented by:

$$E_{surface} = E_{deformation} + E_{forces}$$

[3.1]

where

$$E_{deformation} = \iint \alpha_1 \left|\frac{\partial z}{\partial x}\right|^2 + \alpha_2 \left|\frac{\partial z}{\partial y}\right|^2 + \beta_1 \left|\frac{\partial^2 z}{\partial x^2}\right|^2 + \beta_2 \left|\frac{\partial^2 z}{\partial x \partial y}\right|^2 + \beta_3 \left|\frac{\partial^2 z}{\partial y^2}\right|^2 dxdy$$

[3.2]

represents the deformation energy where the $\{\alpha 1, \alpha 2, \beta 1, \beta 2, \beta 3\}$ represent weighting parameters controlling the elastic behavior of the surface and

$$E_{forces} = -\iint z f(x, y) dxdy$$

[3.3]

represents the data energy derived from a data force given by:

$$f(x, y) = k \left\| z_{data}(x, y) - z_{surface}(x, y) \right\|$$

[3.4]

Fitting of the planar deformable model to the data is accomplished by minimization of the model's energy $\mathbf{E_{surface}}$. Fitting of the model is accomplished iteratively in a dynamic fashion. As can be seen from [3.4], the data force is derived from the distance between the data point in space (derived from the FARO Surgicom) and its point of influence on the deformable model's surface. As the model is iteratively updated, the model is deformed towards the data point, resulting in an increase in the deformation energy $E_{surface}$ (the model is increasingly being deformed) and a decrease in the data energy E_{forces} (the distance between the data point and the model surface is being reduced). Minimization of the model's energy $E_{surface}$, or equivalently the equilibrium of the data and deformation forces, results in the fitting of the model to the surface. In other words, fitting of the

model to the data results in the surface iteratively moving closer to the data points until there is no further change in the model (no change in the derivatives of the displacement direction z with respect to time).

Solution of the deformable model (ie. minimization of $\mathbf{E_{surface}}$) requires that the continuous case presented above be discretized and solved numerically. A finite element representation is necessary and this process will be detailed in the following section.

A finite element representation of the deformable model is attractive for several reasons: it provides an analytical description of the surface, and in contrast with finite difference approaches [52] the resulting surface can be evaluated at any point. Furthermore, finite element techniques in general require fewer discretization nodes (relative to finite difference approaches) which allows for a coarser representation that is faster to evaluate for the same degree of accuracy [51].

In order to apply finite element techniques to the deformable model problem, we begin by selecting a finite element capable of accurately representing the solution to the problem. The complexity of the finite element is the primary consideration since it has a direct bearing on the computational complexity and therefore the time required for the solution to converge. The *shape (*also called *basis* or *interpolation) functions* of the element govern the element's complexity as well as its continuity. Although elements have been formulated with linear, quadratic, cubic and higher orders of shape functions, it is usually the lowest order function giving solutions of sufficient accuracy that is chosen due to the rapidly increasing computational load that the higher order basis functions introduce. The shape of the finite element is often triangular or quadrilateral (rectangular) since these shapes are the simplest subregions into which two and three dimensional regions can be divided. Regular regions such as planes can be subdivided into finite elements by simple parameterization as a function of length and width; irregularly shaped regions may require more sophisticated methods for element tessellation. Regions that are spherical or cylindrical can be parameterized periodically with special treatment at the ends (for example, tessellating a sphere with rectangular elements for the majority of the region with triangular elements on the ends to create a closed surface).

The tessellation of an open, regular region such as the planar deformable model is a simple matter of parameterization, as illustrated in *Figure 3.1*. The planar model can be described as a continuous vector function:

$$u(a_1, a_2)$$
$$0 \leq a_1, a_2 \leq 1 \qquad [3.5]$$

which is approximated by the discrete grid function [52]:

$$u[m,n] = u(mh_1, nh_2)$$
$$1 \leq m \leq M, \quad 1 \leq n \leq N \qquad [3.6]$$

where m and n index the nodes of the elements comprising the surface and where M and N are the number of nodes in the horizontal and vertical directions. The inter-node spacings in the horizontal and vertical directions are h_1 and h_2 respectively.

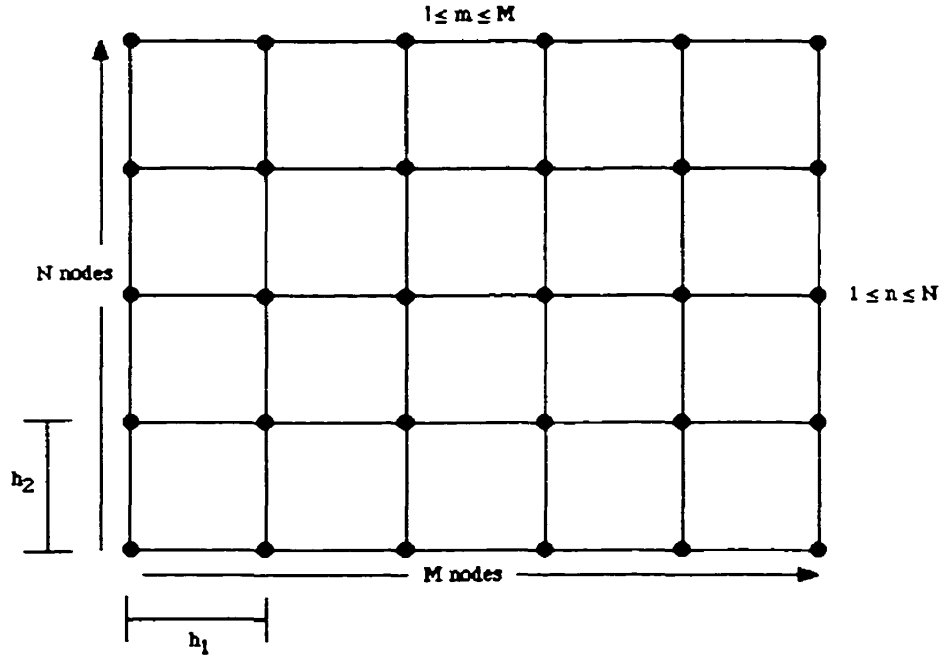

Figure 3.1. Tessellation of an open planar deformable model.

The tessellation of a closed region can be accomplished using periodic functions. A popular closed region in the literature is the superquadric ellipsoid model [53]. This region is tessellated using:

$$x(u_i, v_i) = a_1 \begin{pmatrix} b_1 C_u^{\varepsilon_1} C_v^{\varepsilon_2} \\ b_2 C_u^{\varepsilon_1} S_v^{\varepsilon_2} \\ b_3 S_u^{\varepsilon_1} \end{pmatrix}, \quad -\frac{\pi}{2} \le u \le \frac{\pi}{2}; \quad -\pi \le v \le \pi$$

[3.7a]

where

$$S_w^{\varepsilon} = \text{sgn}(\sin w)|\sin w|^{\varepsilon}$$
$$C_w^{\varepsilon} = \text{sgn}(\cos w)|\cos w|^{\varepsilon}$$

[3.7b]

and $a \ge 0$ is a scaling parameter, $0 \le b_1, b_2, b_3 \le 1$ are aspect ratio parameters and $\varepsilon_1, \varepsilon_2 \ge 0$ are "squareness" parameters. The geometry of the deformable superquadric is shown in *Figure 3.2.*

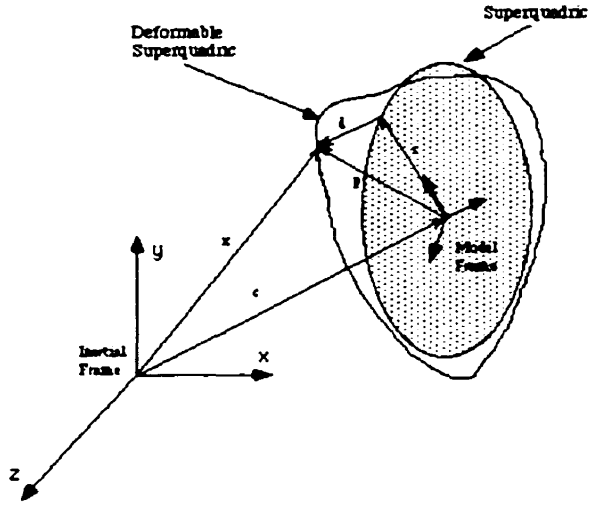

Figure 3.2. Geometry of the deformable superquadric (after [54]).

This closed region model is used in the context of a deformable "balloon" which is defined within a 3D volume either outside or inside the volume of interest. Three dimensional gradient information is used as guidance in the form of data forces to 'deflate' or 'inflate' the model to conform to the volume of interest. These models are most commonly used

for segmentation of volumetric objects from within a 3D volume [54-56]. Some examples of the use of a deformable balloon are shown in *Figure 3.3*.

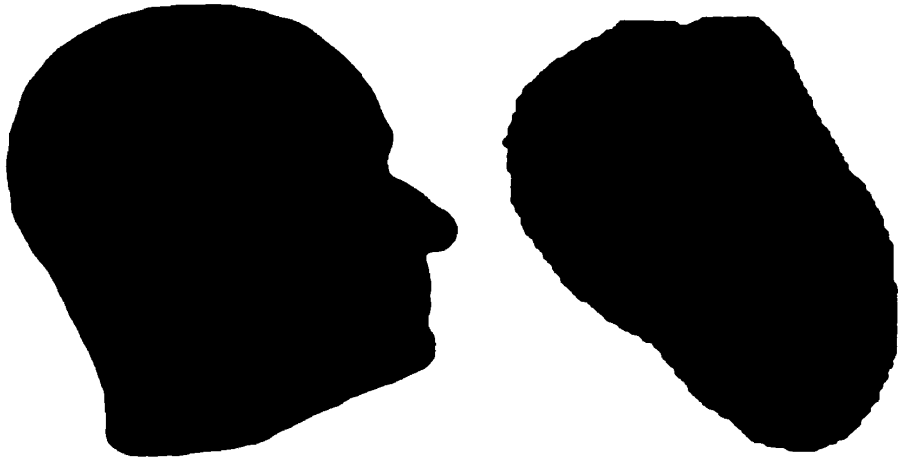

Figure 3.3. Some examples of closed deformable models. The cortical surface shown at left was produced from a deformable balloon model within a volumetric data set using 3D gradient information to conform to the surface [57]. The heart ventricle at right was produced from the use of a balloon deformable model within a 4D data set of the cardiac cycle [56].

Both the closed superquadric ellipsoid and the open planar deformable models were considered for implementation in this project. The use of a closed deformable model such as the superquadric could initially be introduced into a 3D volume and be allowed to conform to the volume of interest at some point before surgery using gradient information inherent within the volume. Data points from the FARO Surgicom could then be used to deform and 'collapse' the model into itself for visualization of intraoperative resection progress. Unfortunately, the collapsing of the model can cause opposite walls to cross each other, thereby introducing a change of topology in the model. A substantial amount of additional mathematical complexity must be introduced to account for these topological changes [58-60] and it was felt that the interactive aspects of the software would be significantly impaired by the additional computation required. The open planar deformable model was found to be the best choice for the intraoperative feedback

application for several reasons. The aforementioned topological changes do not occur when deforming the planar model in a single direction and thus the added complexity to deal with such changes would not be required. The model does not require an initial preoperative step of conforming to a volume of interest: the surgeon defines the planar model's initial location through the acquisition of three points with the FARO Surgicom. The planar model is composed of fewer finite elements due to its smaller surface area in comparison with the superquadric model and as a consequence will require less computation to perform an update when deforming the model. Lastly, the search algorithm required to determine the position on the model's surface where the data point force is applied requires much less computation for the planar model, further increasing deformation update speed.

The finite element used for the planar deformable model in this project is the Bogner-Fox-Schmidt finite element (named for its developers), which is a rectangular, bicubic Hermitian element. This element has been used in elasticity problems and is thus applicable to the deformable model problem formulation. The term *bicubic* refers to the highest degree of interpolation function used in both the x and y extents of the element. The term *Hermitian* refers to elements that utilize the values of both the function and their derivatives at the nodes. Elements of this type are advantageous for computing additional properties of the surface such as curvature. As will be evident in the mathematical development, the Hermitian bicubic element provides C^1 continuity (continuity in the interpolation functions and their first derivatives) due to the fact that energy functional contains second order partial derivatives [51]. These elements are formulated as a thin plates under tension (a simplified formulation of the general shell finite element).

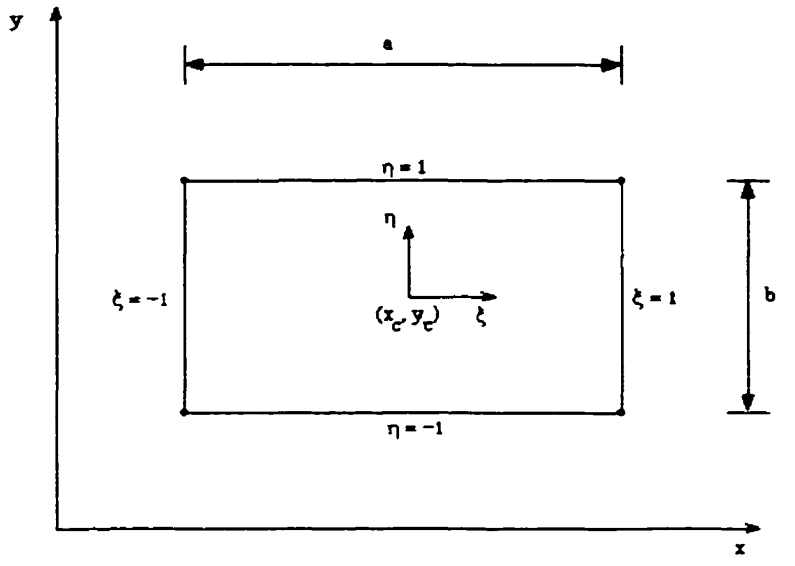

Figure 3.4. The bicubic Hermitian finite element (after [51]).

The bicubic Hermitian element is shown in *Figure 3.4*. The element is described in local coordinates (ξ,η) with respect to the element's centre. The local coordinate system is related to the global coordinate system in which the entire planar deformable model lies by the following relation:

$$\xi = \frac{2}{a}(x - x_{centre}). \quad \eta = \frac{2}{b}(y - y_{centre})$$

[3.8]

where x_{centre} and y_{centre} represent the coordinates of the element's centre and *a* and *b* represent the element's length in the ξ and η directions, respectively.

The z displacement of the element is approximated from the local variables (ξ,η) of the element and the values of z, first partial derivatives with respect to x and y and the second partial derivative with respect to x and y. The approximation, called *the trial function*, is computed as:

$$\hat{z}(x, y) = \sum_{i=1}^{4} N_{1i} z_i + N_{2i} \frac{\partial z_i}{\partial x} + N_{3i} \frac{\partial z_i}{\partial y} + N_{4i} \frac{\partial^2 z_i}{\partial x \partial y} = \sum_{i=1}^{4} N_i(x, y) q_i(t)$$

[3.9a]

where

$$N_{1i} = n_{0i}(\xi)n_{0i}(\eta)$$
$$N_{2i} = n_{0i}(\xi)n_{1i}(\eta)$$
$$N_{3i} = n_{1i}(\xi)n_{0i}(\eta)$$
$$N_{4i} = n_{1i}(\xi)n_{1i}(\eta)$$

[3.9b]

and where the trial function weights $\{N_{1i}, N_{2i}, N_{3i}, N_{4i}\}$ are composed of shape functions $\{n_{0i}, n_{1i}\}$ defined as

$$n_{01}(\xi) = n_{04}(\xi) = 1 - 3\xi^2 + 2\xi^3, n_{01}(\eta) = n_{02}(\eta) = 1 - 3\eta^2 + 2\eta^3,$$
$$n_{11}(\xi) = n_{14}(\xi) = a(\xi - 2\xi^2 + \xi^3), n_{11}(\eta) = n_{12}(\eta) = b(\eta - 2\eta^2 + \eta^3),$$
$$n_{02}(\xi) = n_{03}(\xi) = 3\xi^2 - 2\xi^3, n_{04}(\eta) = n_{03}(\eta) = 3\eta^2 - 2\eta^3,$$
$$n_{12}(\xi) = n_{13}(\xi) = -a(\xi^2 - \xi^3), n_{14}(\eta) = n_{13}(\eta) = -b(\eta^2 - \eta^3)$$

[3.9c]

The $q_i(t)$ are the nodal variables of the i^{th} node in the deformable model mesh and will be described below. Note that the shape functions are expressed as functions of the local coordinates $\{\xi, \eta\}$ and that the shape functions are bicubic. Once the point where the data force is applied to the planar deformable model has been determined in the global coordinates $\{x,y\}$, the point of application can be found in local coordinates using the relation in [3.4]. It is therefore convenient to work in the local coordinate space of the element [51]. Integration over the area of the planar deformable model in global coordinates $\{x,y\}$ can be alternately be expressed in terms of the local coordinates $\{\xi, \eta\}$ as:

$$\iint_{E_j} f(x,y)dxdy = \iint_{E_j} f(x(\xi,\eta), y(\xi,\eta)) \det J d\xi d\eta$$

[3.10a]

where

$$J = \begin{vmatrix} \frac{\partial x}{\partial \xi} & \frac{\partial y}{\partial \xi} \\ \frac{\partial x}{\partial \eta} & \frac{\partial y}{\partial \eta} \end{vmatrix}$$

[3.10b]

and E_j is the region of integration and J is the Jacobian matrix. The above integrals are approximated numerically using Gauss-Legendre numerical integration [51,61].

As can be seen from *Figure 3.4*, each element in the planar deformable model is comprised of 4 nodes. Each node of the element has the following nodal variables or degrees of freedom:

$$q_i(t) = \left[z_i, \left(\frac{\partial z}{\partial x}\right)_i, \left(\frac{\partial z}{\partial y}\right)_i, \left(\frac{\partial^2 z}{\partial x \partial y}\right) \right]^T$$

[3.11]

where z is the displacement of the deformable model and i is the i^{th} node in the mesh. Therefore, each rectangular element possesses 16 degrees of freedom.

The continuous displacement z of the deformable model away from its initially planar shape is approximated by the trial function given in [3.9a]. The energies given in [3.1] can be interpreted as forces [51] through the use of Lagrangian dynamics to yield the second order differential equation:

$$\mu \frac{\partial^2 z}{\partial t^2} + \gamma \frac{\partial z}{\partial t} + \delta E_{deformation} = f(x, y, t)$$

[3.12]

where the second order term represents inertial force due to the mass density $\mu(x,y)$, the first order term represents damping forces due to the damping density $\gamma(x,y)$ and the third term represents an elastic force which resists deformation. The right side of the equation represents the forcing function, the data point force applied to the surface which is acquired intraoperatively from the FARO Surgicom. The data force is a function of the point of application on the deformable model (x,y) and is also a function of time since the magnitude of the force is dependent on the distance between the data point and the surface of the model (see [3.4]). The dynamic fitting of the surface to the data points is governed by [3.12]. It should be noted that the weights $\{\mu,\gamma,\delta\}$ have no correspondence to actual materials since the intent is not to model a real world material but to provide a pliant behavior, such as a 'rubbery' surface. Thus, the values can be appointed arbitrarily.

Substitution of the trial function in [3.9a] (the discrete approximation to the actual displacement z) into [3.12] gives:

$$M\ddot{q} + C\dot{q} + Kq = F_{data}$$

[3.13]

which expresses the dynamic fitting of the surface in terms of the z displacements of the nodes of the deformable model mesh. This is the typical form of the problem that is solved using finite element analysis. The weight M represents the *mass matrix*, C the *damping matrix* and K is the *stiffness matrix*. For applications involving the fitting of data, the computational load can be reduced by simplifying [3.13] to the following:

$$C\dot{q} + Kq = F_{data} \qquad [3.14]$$

The simplification results in a first order differential equation describing a system (the deformable model) which will come to rest when the external forcing function F_{data} vanishes or equilibrates. In the computer implementation the F_{data} are the point forces imposed by the acquired data points. The forces they exert are a function of distance, and decrease as the deformable model approaches the data points. The model comes to rest when a residual has been met (ie. the mean distance between the deformable model's surface and data points). The numerical solution to [3.14] is evaluated using an explicit Euler method [51,61] and the degrees of freedom of the model (z displacement and partial derivatives) are updated according to the formula:

$$q^{(t+\Delta t)} = q^{(t)} + \Delta t(C^{(t)})^{-1}(F_{data}{}^{(t)} - Kq^{(t)}) \qquad [3.15]$$

The time step Δt must be selected carefully [51,61] to optimize computational speed while not introducing numerical instability.

3.5 Algorithm Description

This section describes the execution of the algorithm implemented to provide intraoperative feedback of tissue resection using deformable models. A description of the initial definition of the planar surface with respect to preoperative surface objects is described first, followed by a description of the chain of events which occur when a data point is acquired by the probe tip of the FARO Surgicom to deform the model.

After the registration procedure is complete and preoperative surface objects are loaded into the 3D view to provide context for the deformable model, the surgeon selects

the 'Define Surface...' menu item and acquires three points forming a plane perpendicular to the plane of resection. The fourth point forming the final corner of the initially planar deformable model is generated automatically to lie in the plane of the other three points. The surgeon need not be concerned about the initial size (x and y extents) of the plane since it can be subsequently adjusted using keyboard keys. After the definition of the deformable model has taken place, the resection can begin. The probe tip of the FARO Surgicom is replaced with the rigid attachment of the aspirator and the appropriate offset file for the aspirator is loaded.

When the position is of the aspirator tip is sampled (by the press of a keyboard key), the following series of events occur. The acquisition of a data point is accomplished by locating the aspirator tip at an appropriate site (in the tumour during the resection) and pressing a keyboard key. The newly acquired data point is added to a buffer of data points previously acquired (if any) after a check is made to ensure that the data point lies within the deformable model's boundaries (x and y extents) and that the new data point represents a progression in the deformation (progress in the resection) based on a search for the nearest neighbouring point already in the buffer. It is important that the data point be checked to ensure that its inclusion represents progress in the resection; this allows the acquisition of data points to occur continuously if desired without adversely affecting the accuracy of the deformation of the model. The strength of the data force is computed as a function of the distance between the data point and the surface represented by the deformable model. If the resultant data force is extremely large (ie. the data point lies a great distance from the deformable model), it is set to a maximum value to avoid potential numerical instabilities in the numerical computation. A loop is then performed whereby each data point is iterated in small time steps to numerically solve the differential equation in Eqn. 3.14 to determine and propagate the effect of the data forces on the deformable model and to compute the new positions of the nodes of the mesh representing the deformable model. The stopping criteria for allowing the deformable model system to come to rest is a residual of the difference in the mean distance between the data points and the surface represented by the deformable model. As the surface represented by the deformable model approaches the data points, the strength of the attractive data forces

decreases (since they are defined as a function of distance) and as a result each successive iteration updates the position of the deformable model to a lesser degree.

Within each iteration a routine determines the mesh element over which the data point lies and the location of the data point within that element. The routine computes the local coordinates of the point with respect to the deformable model. Subsequently, another routine computes the z displacement of each mesh node by evaluation of the trial function (Eqn. 9a) using the partial derivatives at that point. The difference between the location of the data point and the surface of the deformable model at that point is then computed; the force imposed by the data point is then distributed to the nodes of the element which contains the data point. The distribution of the point force onto each node is weighted by the interpolation (or shape) functions (see Eqns. 9a and 9b).

3.7 Variables in the Deformable Model

The algorithm implemented for the provision of intraoperative feedback using deformable models has several variables which govern its behavior. An understanding of these variables is necessary in order to optimize the algorithm's behavior for the application of intraoperative feedback and to understand the limitations of the algorithm when real time interactivity is required.

The main variables in the algorithm which influence the deformable model's behavior are:

- the elasticity parameters w_0 and w_1
- the time step (Δt) in the numerical computation
- the mesh density (number of elements)
- the iteration stopping criteria

The elasticity parameters govern the 'physical' behavior of the deformable model (how it moves towards and conforms to the data points representing the resection cavity) while the remaining variables (time step, mesh density and iteration stopping criteria) influence the convergence speed of the deformable model to the data points.

The elasticity parameters (w_0 and w_1) directly influence the behavior of the deformable model. The parameter w_0 controls the membrane term in the surface deformation energy expression ($w_0=\alpha_1$ and α_2 in Eqn. 2) and determines the 'stretchiness' of the model. The parameter w1 controls the thin plate term in the energy expression ($w_1=\beta_1$, β_2 and β_3 in Eqn. 2). The parameters (α_1, α_2, β_1, β_2, β_3) are grouped into the two parameters w0 and w1 according to their influence on the model (the α's weight the first partial derivatives while the β's weight the second order partial derivatives). Using the two parameters, the two extreme behaviors of the deformable model are:

- $w_0 > w_1$, $w_0, w_1 < 1.0$: This produces a 'stretchy' model which is more prone to local deformations, with each point exerting an individual pull on the model
- $w_0 < w_1$, $w_0, w_1 < 1.0$: This produces a smooth and more rigid behaving model more prone to global deformation (movement of the model as a whole). Individual data points work in concert to pull a region of the model

After experimentation with the modelling of different types of cavities (see Chapter 5), a stretchy model setting was chosen for modelling a resection cavity since it has the capability of adhering to detailed shapes and does not smooth edges as in the more rigid setting. The extremes of the model's capabilities are shown in *Figure 3.5*.

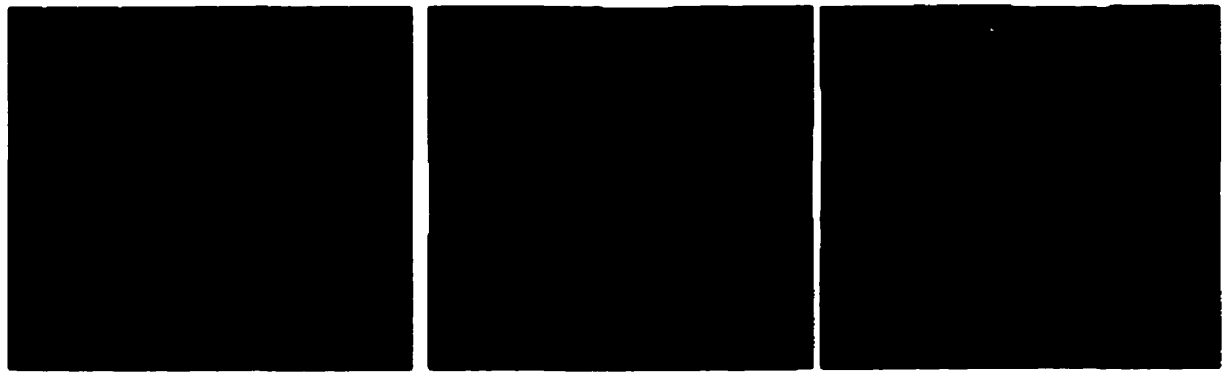

Figure 3.5 Three examples demonstrating the behavior of the model with different values for the weighting parameters w_0 and w_1. At left the model is configured as a smooth and rigid surface ($w_0 < w_1$). At right, the model is configured as very stretchy ($w_0 > w_1$) and a 'cross brace' approach (as in the hull of a ship) is used in acquiring data

to accentuate the local deformation that occurs under these conditions. At centre, the model is configured between these two extremes. Note that the model conforms to the shape while extreme local deformation is minimized.

The time step in [3.15] is set to a static value for the iterative updating. Some experimentation was conducted with the time step in order to optimize it for the real time interactivity required. It was determined that the time step should be set conservatively and remain static to prevent potential numerical instabilities from occurring.

The density of the finite element mesh influences the visual detail that the deformable model provides of the resection cavity but also dictates the speed of convergence of the model to the data points. A mesh with many elements (for example a 50x50 mesh) requires a great deal of computation for each iteration before the iteration stopping criteria is met. With the computing facilities available to the author (SGI Indigo, SGI O2), it was found that a 10x10 mesh provided sufficient detail and reasonable volume estimation accuracy in the validation studies undertaken (see Chapter 5).

The iteration stopping criteria is the means by which the deformable model comes to rest. Although the model is formulated in terms of the minimization of energy, using this scheme as the stopping criteria has drawbacks in terms of computational intensity and convergence to local minima [54]. A more straightforward approach is the use of the mean distance between the surface represented by the model and the user defined data points [54]. This approach has the advantage of low computational complexity and in conjunction with the formulation of the data point force as a function of distance from the surface represented by the model (see [3.4]), gives a robust stopping criteria. When the model has already met data points but needs to continue iterating to meet remaining data points, the data points already met by the model exert a very small force on the model in that area, preventing the model from 'overshooting' those points while it continues to iterate.

3.8 Mathematics of Volume Estimation from Closed 3D Surfaces

In addition to the visualization of cerebral tissue resection provided by the deformable model, a secondary objective of the project was to provide some quantification of the amount of tissue removed. It is usual practice during surgery for the surgeon to roughly estimate the volume of the tumour and the resection cavity through visual inspection. The software developed in this project has the facility to provide volume estimation of the resection cavity as well as volume estimation of preoperatively segmented surface-rendered objects, lending a qualitative aspect to the visualization. The volume estimation method implemented in the project has the capability of providing a much more accurate assessment of volume than is possible through visual inspection alone.

Several methods of volume calculation from images and volumetric data sets have appeared in the literature. Assumptions of parameterized geometric shapes and estimating the parameters [62], the computation of the area of serial sections and multiplication by the slice thickness [62,63], reconstruction of a minimal surface between contiguous slices[62] and estimation of volumes from voxel count or pointlists [63] were all considered and rejected as inappropriate for this project. It should be noted at this point that the BIC program DISPLAY, written by David McDonald, produces a volume estimation of the closed surface segmented from preoperative MRI images by voxel counting. The DISPLAY program was used by the author to segment objects from preoperative MRI data and the volumes estimated by this program were noted and compared with the volume estimation method used in the project software. Close correspondence between volume estimation values was observed.

The procedure used to compute the volume of the resection cavity represented by the deformable model and the preoperative closed surface objects is essentially a discrete numerical integration using the volumes of tetrahedra formed by each triangular facet comprising the surface and an arbitrary point in space as differential elements.

When the planar deformable model is initially defined in 3D space, the initial 'volume' of the surface is computed as the sum of the volumes of the tetrahedral elements formed by each triangular facet of the model and an arbitrary point in space. This initial

'volume' is actually a reference value to subtract from the volume of a deformed surface. When the deformable model has undergone deformation throughout the course of a resection procedure, the volume of the cavity can be computed by carrying out the procedure above (summing the volumes of the tetrahedral elements of the deformed surface) and subtracting the initial 'volume':

$$\mathbf{V(resection\ cavity) = V(deformed\ model) - V(initial\ planar\ model)} \quad [3.16]$$

The current volume estimate of the resection cavity is updated each time the deformable model is updated to deform to the current set of data points. For the volume estimation computation of the deformable model to be accurate, it is important that the deformation be in one direction only. Therefore, care should be taken to initially define the planar deformable model in such a way that the deformation occurs in one direction only. A visual depiction of the algorithm is shown in *Figure 3.6.*

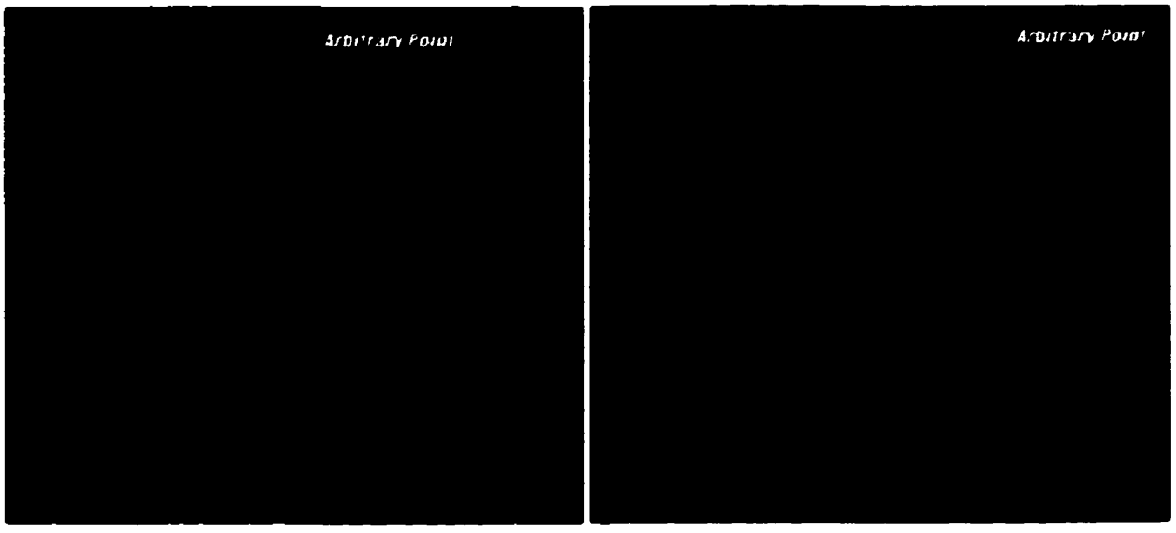

Figure 3.6 Visual depiction of the volume estimation algorithm for the planar deformable surface.

The computation of a volume estimate of the closed preoperative surface-rendered objects segmented from MRI data is slightly more complicated. The 'direction' of the

polygons (must be triangles) must be determined to resolve whether they lie on the 'far' side or the 'near' side of the arbitrary point selected. The polygons in a polygonal representation of a closed surface obey a consistent convention for listing vertices for rendering purposes. Therefore we may say that all polygons face towards the outside of the closed surface and the direction of their normals indicates whether the polygon lies on the 'near' or 'far' side of the surface with respect to an arbitrary point in space. The direction which the polygons face is determined by:

$$SIGN = \bar{N} \bullet ((q-p) \times (r-p)) \qquad [3.17]$$

If SIGN > 0, then the polygon (triangle) with sides PQ and PR (cross product normal to the surface of the polygon) faces the 'near' side and if SIGN < 0, the polygon (triangle) with sides PQ and PR (cross product normal to the surface of the polygon) faces the 'far' side. For example, choosing an arbitrary point at (0, 0, 1000) and projecting a closed surface to the XY (z=0) plane, computation of the above equation with N = (0, 0, 1) will give SIGN>0 for triangles whose normals are directed along the positive z-axis (the 'near' side to (0,0,1000)) and SIGN<0 for triangles whose normals are directed along the negative z-axis (the 'far' side to (0,0,1000)). The net volume of the closed surface object can then be computed as the sum of the volumes of the tetrahedra formed by the 'far' triangular facets and an arbitrary point in space minus the sum of the volumes of the tetrahedra formed by the 'near' triangular facets and an arbitrary point in space:

$$V(\textit{closed surface object}) = \sum(\textit{far tetrahedral volume}) - \sum(\textit{near tetrahedral volume}) \qquad [3.18]$$

The accuracy of the volume estimation algorithm is of course dictated by the number of discrete tetrahedra used. This is directly influenced by the mesh size of the deformable model and the number of polygons in the representation of the closed surface objects.

Details of the volume estimation accuracy are reported in Chapter 5. A visual depiction of the algorithm is shown in *Figure 3.7*.

Figure 3.7 Visual depiction of the volume estimation algorithm for closed surfaces.

As discussed earlier, the BIC programs DISPLAY and TRIANGULATE_POLYGONS were used to generate a triangle-only polygonal representation of closed surface object from preoperative MRI data. The reason for a triangular mesh is clear; triangles are required for the volume estimation algorithm implemented in the project.

Chapter 4

Implementation

4.1 Introduction

This chapter deals with the implementation of a deformable model in computer software for visualization and quantification of cerebral tissue resection. The mathematical formulation of the deformable model and its finite element origins were presented in Chapter 3.

A description of the use of the project for intraoperative visualization in the OR is presented, followed by the details of the construction and calibration of the aspirator connection to the FARO Surgicom. Finally, the integration of the project into VIPER, our laboratory's IGNS development platform, is presented.

4.2 Program Description

The project described in this thesis was developed in the Image Guided Neurosurgery Laboratory at the Montreal Neurological Institute, McGill University, as a part of ongoing efforts to design and implement modules within VIPER, the laboratory's IGNS development platform. The VIPER platform employs Silicon Graphics O2, Indigo and Indy workstations running the IRIX (SGI UNIX) operating system. These workstations provide specialized graphics engines that provide the capabilities required for this type of work. Positional information for probes and other tools is provided by a FARO Surgicom articulated arm, which is used for registration, intraoperative surgical planning and navigation and for acquisition of data force points for this project. The VIPER software is written in object-oriented fashion in C++, using Motif libraries for the graphical user interface (GUI) and OpenGL graphics libraries as primitives in the graphical display. The project contributed several new C++ objects, such as SurfaceObject and DeformableSurfaceObject, to the VIPER source code. Many other existing VIPER objects were modified accordingly as well to accept the deformable

surface implementation and expanded as necessary. The SurfaceObject C++ object contains the necessary functionality for surface rendering 3D objects from segmented MRI data and providing translucency, lighting and other associated rendering functions. The 'machinery' of the deformable model is primarily contained in the DeformableSurfaceObject C++ object. This object contains a great deal of functionality, from the user definition of the deformable surface model in 3D space with data acquired from the FARO Surgicom, to drawing and rendering the deformable surface model in the 2D/3D views to the imposition of data forces to deform the model. The complete algorithm used for the implementation of the deformable model was presented in Section 3.6.

The development of the project came at a time during which VIPER was in its initial stages, and several key contributions from this project were particularly significant in its evolution. The implementation of the 3D view within VIPER, surface rendering of objects segmented from preoperative MRI data, display of surfaces with polygonal skeleton or translucent qualities, and the provision for real-time probe tracking as an intraoperative data acquisition tool for deforming surfaces or even drawing in 2D/3D were contributions to VIPER afforded by the project described in this thesis.

4.3 OR Protocol for Intraoperative Visualization Using the Deformable Surface Model

This section describes the use of the intraoperative visualization and quantification software in the operating room during a procedure involving cerebral tissue resection. Although the author did not have an opportunity to validate the software in an OR setting, this section provides a typical sequence of events for its use. A detailed description of the work-up of a patient for a surgical procedure is not presented here; only the details involving the visualization software are elucidated. A complete account of a patient experience of the neurosurgical process is presented in Chapter 6.

4.3.1 Preoperative Preparation

In the preoperative period, a series of imaging studies are conducted to provide the surgeon with anatomical, functional and vasculature information. The number and type of

imaging modalities used are dictated by the procedure to be performed. Usually preoperative MRI data are used intraoperatively for surgical guidance. This data is used in the IGNS computer display and provides the context upon which the deformable surface model is superimposed. The resection visualization can then be seen relative to anatomical structures such as tumour margins. Additional modalities can provide additional information to allow the surgeon to ascertain the proximity of the resection cavity to functional and vascular areas.

Relevant three dimensional objects, such as the cortex, tumour and ventricles are segmented from the preoperative MRI data to provide context for the surface rendered version of the deformable model. Segmentation of objects from volumetric data sets is accomplished using DISPLAY to produce a polygonal representation of the segmented object and TRIANGULATE_POLYGONS is used to reformat the surface produced to triangles only (required for the volume estimation algorithm implemented in the project). The programs DISPLAY and TRIANGULATE_POLYGONS were developed by David McDonald for use at the Brain Imaging Center (BIC) of the Montreal Neurological Institute (MNI). It should again be noted at this point that DISPLAY has the ability to calculate the volume enclosed by a region segmented from the preoperative MRI data set by counting voxels. This function of the software can provide good accuracy but the accuracy itself is a function of the segmentation produced and the thresholds selected to fill the region. 'Label objects' can also be constructed with DISPLAY; these objects are essentially 3D sub-volumes that have been filled with a solid colour. They can be used in VIPER's 2D views to highlight a specific region, such as a tumour.

4.3.2 Initial Intraoperative Procedures

As the anesthetized patient is brought into the OR suite, the IGNS system is simultaneously set up by a computer technician. Volumetric data sets acquired during the preoperative period are loaded either via magnetic tape or network connection. The IGNS software (such as VIPER) is launched and the 2D and 3D views are created. The MRI and other required data sets are loaded for the triplanar 2D views and surface rendered objects are loaded for the 3D view. The data that are loaded into the 2D and 3D views provide the context for the deformable model to be superimposed upon during the surgical procedure.

Adjustment of 2D viewing parameters, such as selection of the opacity, window and level to render the MR volume translucent and to optimize contrast is then performed. Secondary volumes from PET or fMRI are often superimposed on the MRI slice data to provide functional information. The patient's head is fixed in the Mayfield clamp and the FARO Surgicom is put in place. The registration procedure is then performed to relate the patient and image spaces.

4.3.3 Intraoperative Tissue Resection Procedure

Once registration of the patient space to the image space has been performed, the probe is used intermittently through the initial stages of the operation for localization of structures and for checking registration accuracy after the skin incision (against the skull) and after skull removal (against the dura). After the skull and dura are opened, the approach is made to the area of the tumour, avoiding any areas of vital brain function and vasculature. In many neurosurgical procedures, the approach involves a linear incision made at the cortical surface of the brain. The incision is gently separated and the approach to the pathology is made. An aspirator (suction device) is often used to perform the resection of tissue. It should be noted that since the aspirator, or CUSA as it is known to the neurosurgeons, is very commonly used for tissue resections, the intraoperative feedback provided by the project can find utility in a considerable number of neurosurgical procedures. When the surgeon is ready to begin resection, he/she defines three points delineating a plane perpendicular to the resection work (ie. the aspirator works through this plane). It is suggested that the surgeon attempt to define the three data points as a square to ensure that the plane can be decomposed into approximately square finite elements. The software uses the extents of the plane defined by the user to construct a rectangle in space; the fourth point is automatically generated to produce a rectangle with orthogonal sides. The defined plane can be enlarged or reduced using keys on the computer keyboard to adjust its size relative to other objects in the 3D view. This allows the surgeon is define a small plane that is perpendicular to the resection work without concern for its initial size. It is suggested that the size of the surface be adjusted so that its extent encompasses the pathology and allows for some area on the periphery for

deformation purposes. A conceptual illustration of the definition of an initial plane is presented in *Figure 4.1*.

Figure 4.1 Conceptualization of the process of defining an initial plane with respect to the patient's head and tumour.

Once the plane has been defined, the probe tip of the FARO Surgicom can be interchanged with the aspirator tip. If required, a predeformation step can be carried out to adhere the surface to the cortex as described in Section 4.4.1.2. The resection then proceeds as usual, acquiring data points corresponding to the location of the aspirator tip when it is extended into the pathological area to remove tissue. The acquisition of points is performed by pressing a button on the computer keyboard while the aspirator tip lies in the resection cavity. Other possibilities for the acquisition of points include the use of a foot pedal or a button on the aspirator itself (detailed user interface issues were not focused on in the project). Alternately the software has the capability of continuously acquiring data points; the algorithm includes a provision for ignoring data points that do not represent progress in the resection cavity. The surgeon has the capability of saving the data points used to produce the resection cavity visualization at any time during the surgical procedure, enabling it to be recalled after the procedure with different mesh densities or surface properties if desired. A buffer of current deformation points is maintained at all times, reflecting the current state of the resection. Each data point exerts a force whose magnitude is a function of its distance from the deformable model; as the surface approaches the data point, the magnitude of the force produced by the point decreases. This provides a convergence of the surface to the data points. Deformation of

the deformable model to the data points can be accomplished after acquisition of each point, but it is usually better practice to update the visualization of the resection cavity after gathering a number of points. In this way a break or other convenient point in the procedure can be used to update the model, since updating the model with each new point requires iterative calculation that prevents the IGNS display from updating for several seconds. The result is a surface displayed in 3D space representing the current state of the resection that evolves throughout the procedure to provide the surgeon with an intraoperative visualization of resection progress and its location with respect to the important non-pathological areas. After each re-calculation of the deformable model, a current volume estimate of the resection cavity is displayed in the UNIX window.

Observations made from the validation studies presented in Chapter 5 suggest several recommendations that can be made to produce a more accurate deformation result. During a resection, the surgeon should define the upper edges well when traversing into a cavity (ie. the edges of the cavity should be well defined with relatively many data points). This prevents the deformable model from being 'pulled' away from the upper edge of the cavity when deforming into it. Deforming the model into a resection cavity can be conceptually thought of as pinning a rubber sheet into a hole. One wishes to pin the rubber sheet around the upper edges of the hole and also to pin it to the contours of the sides and bottom of the hole so that it adheres to the walls and accurately represents the hole. It is the margins of the resection cavity that are ultimately delineated with the model. In fluid filled cavities, points on the walls are acquired to visualize the cavity.

Care should be taken when the initial plane (perpendicular to the resection) is defined; it should be defined in such a way that the deformation will be entirely unidirectional. This prevents buckling of the deformable model back upon itself, pulling of the model away from data points and allows the volume estimation algorithm to calculate the volume estimate correctly.

It should be noted that the use of high density of points in a given area effectively weights the region more heavily when deforming the model. This can be advantageous in situations where there is a deep crevice or several steep walls comprising the cavity. Use of a larger number of data points in these areas will draw the deformable model more strongly to these regions. The point replacement portion of the algorithm prevents a large

build-up of points in any one region and replaces older data points with newer points reflecting further progress in the resection extent. Areas with greater data point density will draw the deformable model with greater strength relative to areas with less data point density, but the overall deformable model will converge to all data points after a sufficient number of iterations have been performed.

4.3.4 Postoperative Procedures

At the conclusion of the surgical procedure, the data points delineating the final extent of the resection cavity can be saved to a data file for later retrieval. In this way, the surgeon can view his/her work after the fact and evaluate the extent of the resection performed. Since the time required for deformation is not as critical in the postoperative period, the data gathered during the procedure can be used to deform a more finely tessellated mesh (relative to that used during the procedure) to give a highly detailed picture of the resection cavity. Postoperative viewing of the resection can also be useful to neuropsychologists in correlating the extent of resection with observed symptom reduction and/or newly developed neurological deficits incurred as a result of the surgical intervention.

4.4 Intraoperative Visualization Tool within VIPER

This section describes the intraoperative feedback developed in this project as it appears within VIPER, our multimodality neurosurgical planning and neuro-navigational development platform. The objective is not to describe in detail VIPER itself, but to detail the intraoperative feedback facility and how it is integrated into VIPER. A good discussion of the VIPER platform can be found in [64].

4.4.1 3D Display

The 3D view presented in *Figure 4.2* is typically one of the four views presented in the VIPER display panel. It can be used for variety of purposes, such as surface rendering of preoperative surface objects segmented from MRI data and 3D representations of virtual tools such as the leukotome [64] for thallidotomy and pallidotomy procedures. The 3D representation of the deformable model used for intraoperative feedback is rendered in

this 3D view, along with relevant preoperative surface renderings to provide context. An example of a typical deformable model display is illustrated in *Figure 4.3*. The deformable model can be user defined to have a mesh or solid representation (during iterations the model is drawn as a mesh to speed display). During the acquisition of data points, a cursor provides visual feedback to the holder of the probe tip/aspirator of its position relative to structures. When data points are acquired they appear as red points within the 3D space. When the deformable model is updated (with the press of a keyboard key), the proximity of the model to the data points can clearly be seen. The opacity values of the preoperative surface objects and the deformable model can be adjusted by the user to optimize the visualization. The 3D scene can contain any combination of preoperative surface objects, the deformable model, 3D tool visualization and tag points. The scene itself can be viewed from any perspective through rotation of the scene with the mouse. During rotations to alter viewing perspective, the scene is redrawn with a fraction of the total number of polygons in the scene, again speeding the display and user interaction. Hidden surface removal is employed to reduce the number of polygons rendered and in general preoperative surface objects are represented with an upper limit of 8000-10000 polygons in order to maintain adequate interactivity. The 3D view is given simple lighting and a perspective projection to aid in discerning relative positions of objects in the regular monocular view. The VIPER platform also supports stereoscopic viewing (see below).

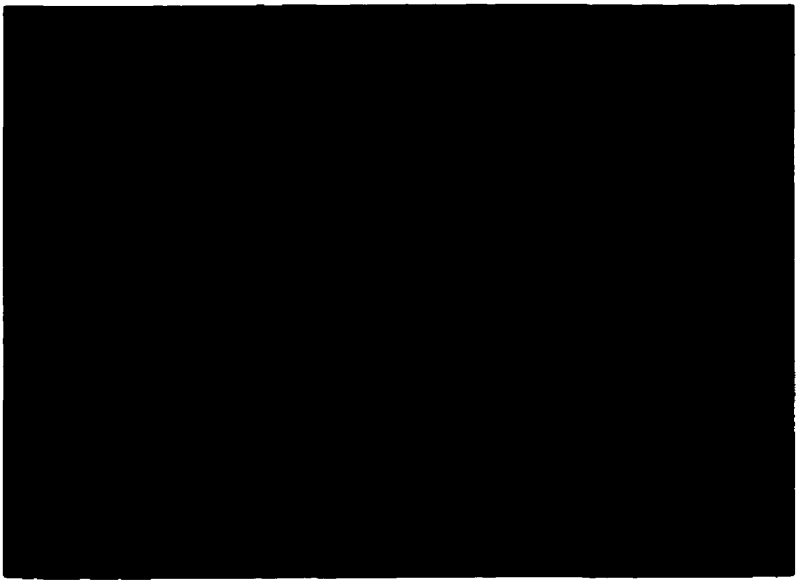

Figure 4.2 VIPER screen showing deformable model screen.

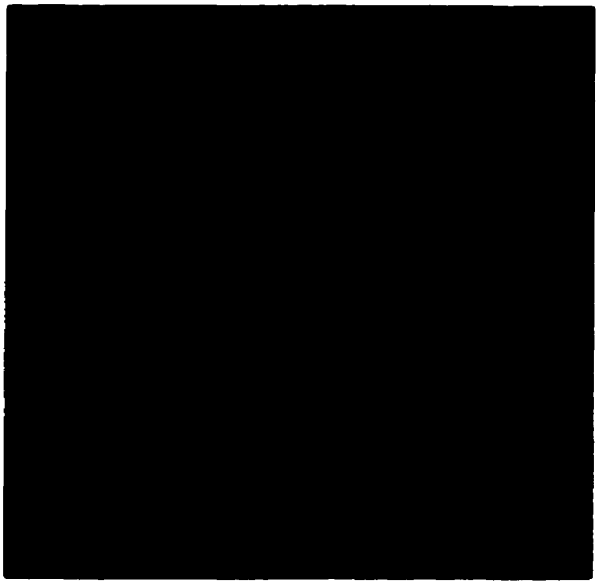

Figure 4.3 Typical deformable model display.

4.4.1.1 Intersections of Model with the Orthogonal Planes

The VIPER platform display panel typically presents four views to the surgeon: three orthogonal triplanar 2D views (sagittal, coronal and axial) and a 3D view. During the acquisition of data points for deformation of the model during a resection (or while the FARO Surgicom probe tip is active in general), the 2D triplanar views present preoperative image slices which intersect the point at which the probe/aspirator tip is currently located. To further aid the surgeon in fusing the relationship between the 2D and 3D views, a visual demarcation of the locations of the orthogonal images planes on the deformable model is provided. Red, green and blue lines on the deformable model surface indicate where the coronal, sagittal and axial image plane would intersect the model in real time while the probe/aspirator tip is active (ie. acquiring data). *Figure 4.4* illustrates how this is represented in the VIPER 3D view display.

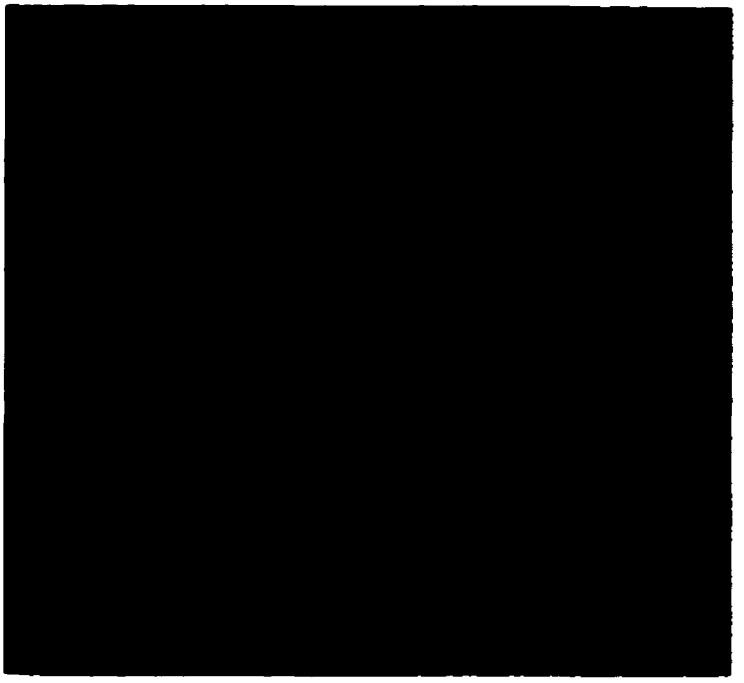

Figure 4.4 Visual demarcation of the current locations of the orthogonal planes intersecting the deformable model. The intersections are depicted as red, green and blue dotted lines as seen above.

4.4.1.2 Pre-Deformation to the Cortical Surface

In certain surgical procedures the cortex overlying the pathology is removed in addition to tissue below the surface. In order to account for this portion of the resection in the visualization, it is required that the deformable model initially conform to the cortical surface topology prior to resection. This is easily accomplished using the following procedure. Before resection is carried out the overlying cortex is first digitized by carefully acquiring data points on the cortical surface using the FARO Surgicom probe tip; the model is then deformed to the cortex. The number of data points acquired and therefore the degree of detail captured is decided by the surgeon; generally three to four minutes are required to acquire points representing the ridges and valleys of sulci. In addition the surgeon must take care with the probe tip during acquisition not to damage tissue. Alternatively the surgeon might outline the cortical surface without actually touching it to move the deformable model close to the surface without risking damage from the probe tip. An example of the pre-deformation to a cortical surface constructed

from a brain mold using plaster of paris is shown in *Figure 4.5*. After pre-deformation to the cortical surface has been accomplished, the state of the model represents a zero initial volume and further deformations begin the accumulation of the resection cavity volume estimates. In the ideal case, the acquisition of data representing the cortical surface by an alternate means such as a laser rangefinder would aid in providing an extremely accurate representation of the surface, but the use of the probe, while not ideal, is adequate for this purpose.

Figure 4.5 Pre-deformation to a plaster mold of cortex. The model at right was generated from the heart-shaped region at left.

4.4.2 2D Display

Although the deformable model is primarily viewed in the 3D view of VIPER's four view display panel, information is provided in both the 2D and 3D views to aid the surgeon in fusing the 2D information provided by the orthogonal images with the 3D view of preoperative surface objects and deformable model. The visual representation of the deformable model in the 3D view of where the 2D image planes intersect the model has already been discussed above. The propagation of information from the 3D view onto the 2D views is also implemented, in the form of cross sections of the 3D deformable model superimposed on the 2D image slices. It is important to propagate the deformable model information onto the 2D image slices since it is these slices upon which the surgeon most relies for the purposes of surgical planning and intraoperative neuro-navigation. Since the deformable model exists as a finite element representation, the surface it represents can be evaluated at any point. This allows the user to specify a location in 3D space with the FARO Surgicom probe/aspirator tip or click within the 2D image planes with the mouse

cursor. The point selected through either means is used to define an intersection point of three orthogonal planes specifying the region of interest. The intersection of these planes with the surface represented by the deformable model is determined and the intersections are superimposed on the 2D image slices as yellow lines, and in the 3D view as red, green and blue lines on the model. The intersections are determined from a fine sampling of the deformable model at many points and checking whether these points intersect the orthogonal planes defined by the user defined location point. Points are utilized rather than attempting an analytical solution since the deformable model may be highly convoluted through the deformation process and therefore a plane may pass through the model at several points. Some typical examples showing the intersection of a point of interest with the deformable model and the cross-sections generated in the 2D and 3D views are shown in ***Figure 4.6***.

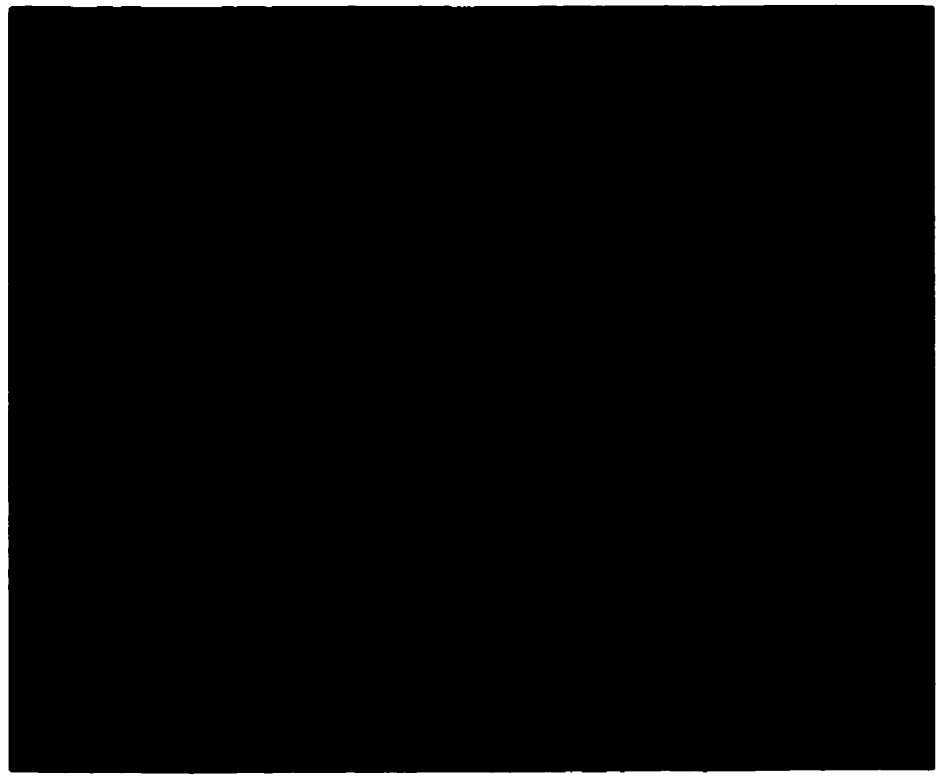

Figure 4.6 The display of cross-sections representing the intersection of the deformable model with the orthogonal planes.

Displays of the cross-sections of preoperative surface objects are also possible in the 3D views. During the segmentation and production of polygonal representations of the preoperative surface objects from preoperative MRI data using the program DISPLAY discussed earlier, a solid representation of the object may also be produced as a sub-volume. This sub-volume may be loaded into VIPER as a 'label object' and superimposed onto the 2D image slices to produce a solid cross-section of the preoperative surface objects.

4.4.3 Volume Estimation of 3D Closed Surfaces

Volume estimation of the preoperative surface objects as well as the deformed model representing the resection cavity is provided by the project as well. This lends a quantitative aspect to the visualization achieved. This computation is performed as described in Chapter 3. Computation of volume estimates of the preoperative surface objects occurs automatically when they are loaded into VIPER, with the result being displayed in the IRIX window from which the VIPER application was originally launched. Computation of volume estimates of the deformable model throughout a resection procedure occur after each series of iterative updates is completed. The accuracy of the volume estimates is reliant upon the density of data and the fineness of the mesh used to represent the model; accuracies within 5% were achieved in validation studies using a mesh fineness and data point density and number representative of what might be used

during an actual procedure (for example, 10x10 mesh with 800 data points). Details of the validation studies are presented in Chapter 5.

4.4.4 Stereo Capability

The VIPER platform supports the ability of the surgeon to observe the 3D view stereoscopically. Although the 3D view provides many depth cues (perspective projection, lighting effects, occlusion and movement of the scene via mouse control), it is still inherently a monocular image. Due to these limitations and the requirement that the surgeon be intimately familiar with the proximity of structures, a stereoscopic viewing facility was developed, using active glasses (CrystalEyes, Stereographics, San Raphael, CA) with liquid crystal 'shutters' synchronized to the frame rate of the computer display. The basic technique allows for each eye to see a slightly different (rotated) image to allow the visual cortex to form a binocular image of the scene. This facility within VIPER allows for further realism and provides the surgeon with more information regarding the 3D relationships between structures.

4.5 Real Time Interactivity Issues

The primary objective of this project was to design and implement software to perform intraoperative visualization and quantification of tissue resection in real time. This section describes the factors that influence the interactive nature of the software and the trade-offs involved in achieving this.

The variables in the deformable model were discussed in Chapter 3. The relevant variables which influence the interactive nature of the software are:

- number of data points involved in deforming the model
- the fineness of the finite element mesh representing the deformable model
- the magnitude of the data forces and iteration stopping criteria

In addition, other factors that influenced the speed of the software include the drawing and rendering routines and the manner in which the software is used. These factors are discussed below.

The number of data points used in the deformation directly influence the speed of deformation since the iterations of the required computations are necessary for each data point acquired. To reduce this computational load, the data points are stored in a finite, 1000 point buffer. In addition, data points are analyzed to ensure that they represent progress in the resection and that they lie within the boundaries of the deformable model. These measures were sufficient to keep the number of active data points (points that influence deformation) within the bounds of the buffer size.

The number of elements comprising the finite element mesh representing the deformable model demonstrate the major trade-off involved in the use of this software for real time application: deformation speed vs. rendered detail. The use of a dense mesh (50x50 or 100x100 or example) applied to a small physical area (2 cm^2) will result in the resolution of considerable detail of the resection cavity. However, the use of such a mesh is prohibitive from the standpoint that the computational load incurred is substantial – deformation of such a mesh by even a few data points is quite slow. A trade-off is to use a coarser mesh which is still able to represent adequate detail (and provide a reasonably accurate volume estimate) whilst maintaining a short deformation time. For practical purposes a mesh of 10x10 to 25x25 representing a small physical area (a realistic assumption in neurosurgical procedures) is adequate to accomplish the aforementioned goals of detail (and accurate volume estimate) and short deformation time using the hardware available to the author (SGI Indy, Indigo, O2).

The magnitude of the data forces and the iteration stopping criteria are also factors in deformation speed. The use of an extremely large magnitude data force can result in numerical instabilities so a limit was imposed. The magnitude of the data force is large enough to pull the deformable model strongly and quickly (large displacements per iteration). Since the magnitude of the data force is formulated as a function of the distance between the deformable model and the data point, as the model approaches the data point the change in displacement per iteration becomes smaller and convergence of the model to the data points slows. In conjunction with a small residual representing the mean distance between the model and data points, a large number of iterations may be required to meet the criteria. Therefore, a large magnitude limit was set on the data force (though small

enough to prevent numerical instability) and the residual was set to a realistic value determined through experimentation in the validation phase.

Optimization of the drawing routines used in rendering the 3D scene is also important to the speed of the software. To increase the speed of rendering the scene, several measures were taken. The preoperative surface objects (there can be several in the 3D scene) required a large number of polygons for realistic presentation. The number of polygons for each object was limited to less than 8000 to maintain drawing speed. During view manipulation of the 3D view with the mouse, a sparse polygonal representation of the preoperative surface objects is used to enhance drawing speed. During the deformation of the model, a mesh representation is used to reduce the amount of computation required. Only once the deformable model has converged is the lighting and shading applied. The lighting and shading models used in the surface rendering are simple and do not require extensive computation and hidden surface removal is employed on all objects in the 3D scene to reduce the number of polygons that are required to be drawn.

Finally, the method in which the software is used has an impact on the speed of the intraoperative feedback. Computing the deformation of the model after the acquisition of each data point is inefficient and impractical. Instead, a better approach is to acquire several points as the resection proceeds and perform deformation of the model on a regular basis, mimicking the work of the surgeon resecting tissue a small amount at a time.

In summary, the following recommendations can be made on the use of the software for successful real time interactivity:

- preoperative surface objects should be rendered with 8000-10000 polygons to ensure adequate speed of movement and rendering of the 3D scene
- the deformable model should be tessellated into a 10x10 to 25x25 finite element mesh for acceptable deformation speed (~20-30 seconds)
- use of a realistic residual for iteration stopping criteria and a large magnitude data force
- deformation of the model in a periodic fashion (not after each acquisition of a data point)

Chapter 5

Validation

5.1 Introduction

The focus of this chapter is the validation of the deformable model as a viable tool for intraoperative feedback: to investigate the capabilities of the deformable model in visualizing and quantifying tissue resection. Experimentation with the deformable model software allowed for investigation into variations in the model parameters such as mesh size, deformation time, number of data points, weighting factors w_0/w_1 and the magnitude of the data force applied to deform the mesh. These variations allowed the author to gain a thorough understanding of the behavior of the model and therefore to 'fine tune' it for optimal representation of resection cavities and calculation of volume estimates. The validation studies were conducted in three phases, with each subsequent phase being a superset of the one preceding it leading to a full mock resection trial with registration to an MR phantom. Each validation phase describes the apparatus used in the experiment, the procedure followed, the parameters varied and results for the visualization and volume estimate of the resection cavity.

5.1 Phase I - Investigation of Modelling Capability

5.1.1 Experimental Procedure

The first phase of the validation studies was designed to investigate the capabilities of the deformable model in assuming the shape of different cavities. Cavities were constructed as detailed below. The results of the cavity modelling were compared on two bases: in qualitative terms (close visual correspondence between the deformed model and the cavity) and in quantitative terms (accuracy of volume estimate). Variations in the model parameters were conducted to ascertain the behavior of the deformable model under various conditions and the relative influence of each of the parameters in determining the outcome. The parameters varied during the course of the trials in this phase (and indeed all phases) were:

- the mesh size (the number of elements in the mesh), which influences the time required for deformation and detail resolved
- number of acquired data points, which influences the detail captured by the deformed model in representing the cavity
- weighting parameters w_0 and w_1, which influence the rigidity of the deformable model (the ease with which the model deforms due to data forces)

The results obtained in each phase of the validation studies are detailed in the following sections.

5.1.2 Construction of Cavity Model

The model cavities were initially constructed from modelling compound (ie. Playdoh) and subsequently from plaster of paris molds to allow greater repeatability. The cavities were made with irregular, non-symmetrical shapes to allow their orientation to be clearly distinguished in VIPER's 3D view. The cavities were also designed to be 'top-down', meaning that the cavities were able to hold a quantity of water, allowing for the measurement of their volume using a graduated cylinder. A trial involving a pre-deformation to the cortex (that is, deforming the model to the cortex as discussed in Chapter 4) was also carried out using a plaster cast of a brain mold.

5.1.3 Modelling Capability

During this initial phase of the validation study, much experimentation was undertaken in the construction of various cavities to employ in investigating the modelling capabilities of the software as well the correlation between different parameter settings and the modelled result. Measurement of deformation time with varying mesh size and measurement of deformation time with number of data force points was investigated to develop recommendations for the software's use. In order to acquire data for these cavities, a probe tip of the FARO Surgicom was used to touch the walls of the cavity and data points were acquired at many points. The usual practice in digitizing the cavities was to begin by defining the plane perpendicular to the extent of the cavity and outlining the upper edge of the cavity with a number of data points. Additional points representing the

cavity were then acquired by following the contour of the cavity walls, often employing a 'cross brace' approach' – by forming 'ribs' along the walls for the model to conform to. The majority of the points acquired were placed at the upper edge of the cavity, at the bottom of the cavity and in location where more local detail was desired. A much smaller number of points was used along the walls of the cavity. In each case approximately five minutes were taken to acquire the data (usually 500-1000 data points used).

The determination of the best w_0/w_1 weighting for the most visually accurate modelling result was found through experimentation to be the combination which produced a 'stretchy' surface (see Chapter 3). Recall that a 'stretchy' surface is more greatly influenced by local deformations (ie. the influence exerted by a single point data force) than is a 'rigid' surface. Such a 'stretchy' surface is more appropriate for fitting to local detail such as sharp ridges and cracks. A relatively coarse mesh (10x10) was found to be suitable for quickly fitting the model to the general shape of the cavity; a finer mesh (50x50) is slower to converge but provides greater local detail. Some example images from the Phase I trials are illustrated in *Figure 5.1* and *Figure 5.2*.

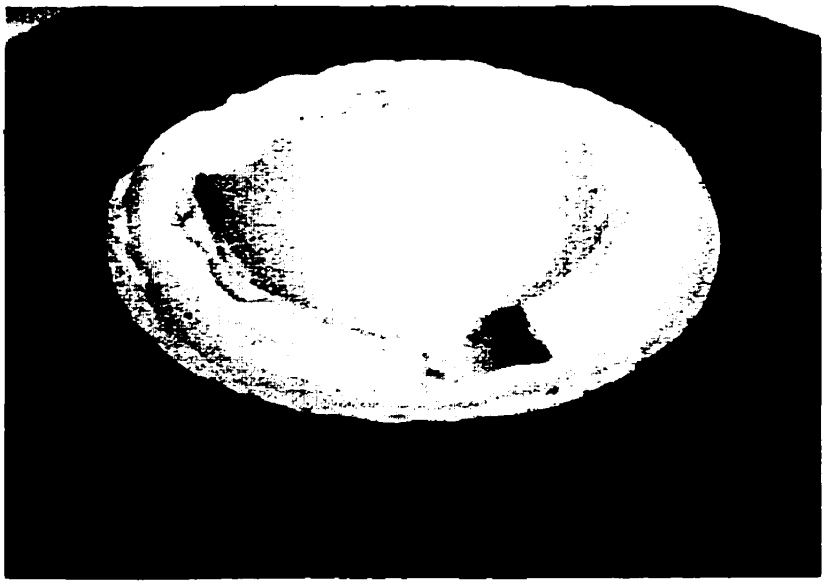

Figure 5.1 Typical plaster of paris cavity used during Phase I investigations into the modelling capability of the deformable model.

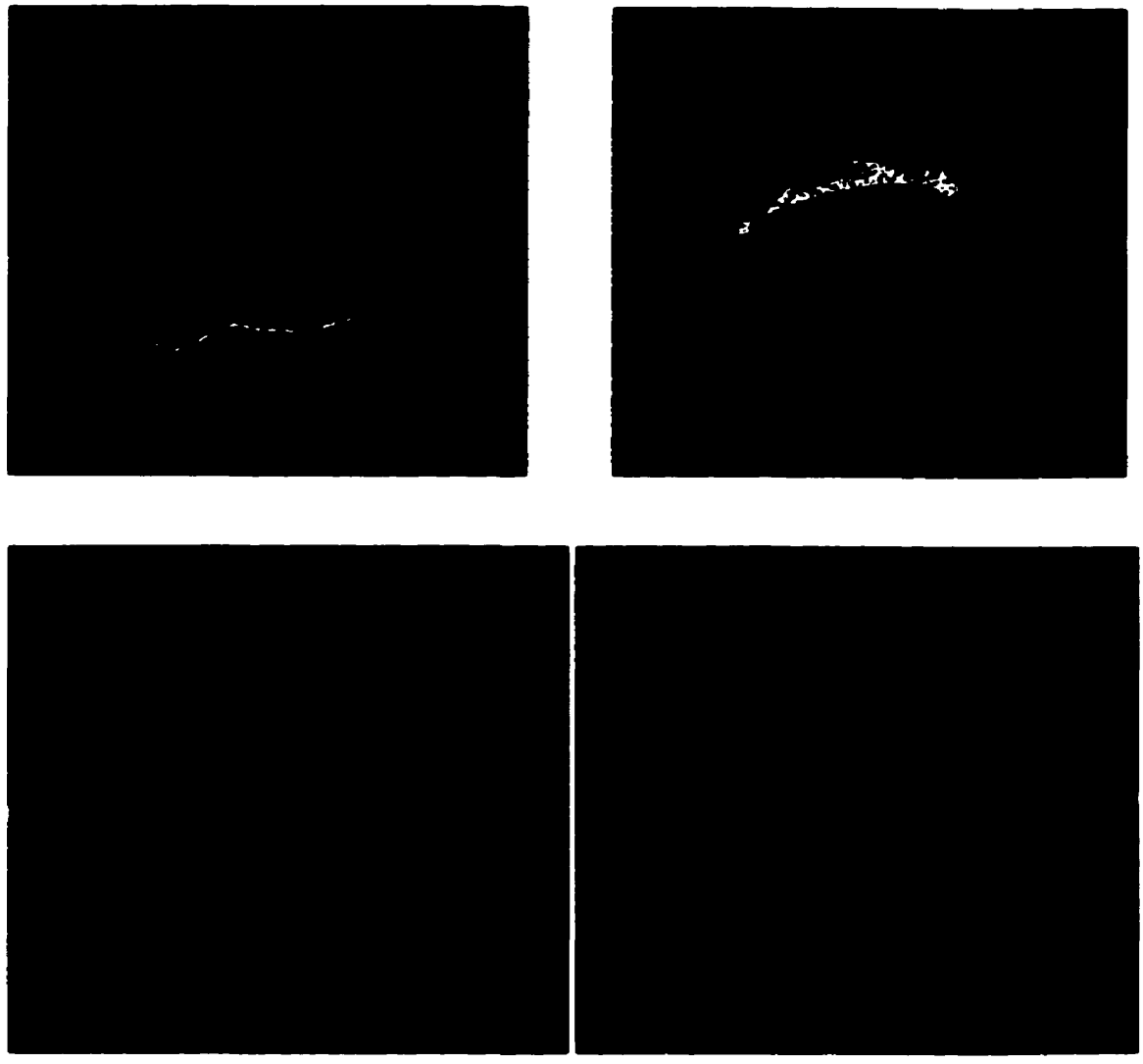

Figure 5.2 Modelling of the plaster of paris cavity in Figure 5.1. This model was produced using a 50x50 mesh, 794 data points and 1000 iterations. Note the data points on the model and how a 'cross brace' approach was used on the cavity walls to conform the model to the cavity.

Modelling of different cavities was undertaken with differing numbers of data points and mesh densities, ranging from as few as 250 data points and a 10x10 mesh to 1000 data points and a 50x50 mesh. Obviously, a larger set of data points or a finer mesh resulted in longer deformation time. The deformation times ranged from the order of seconds for a coarse mesh or a small set of data points to 1-2 minutes for a dense mesh (50x50 for example) with a relatively large number of data points. From the

experimentation conducted in this phase of the validation study, a general recommendation for relatively short deformation time is to use a 25x25 mesh with an active buffer of 500-750 active data points (that is, the most recent data points reflecting the current state of the resection).

5.1.4 Volume Estimation Capability

The cavity models used in Phase I were constructed to allow for the determination of volume using a graduated cylinder and water. In this way, the volume estimate computed from the model could be compared against an independently determined and reasonably accurate value.

The following tables represent typical results obtained during the experiments. *Table 5.1* details results obtained using a small beaker placed open end down on a flat surface. The initial plane was defined as a square outside of the beaker. Acquisition of data points began with outlining the outer lip of the face down beaker, which was touching the flat surface, and then outlining the bottom of the beaker and acquiring interior points. The deformable model was required to conform to the very steep walls of the beaker (something very difficult to accomplish with a simple b-spline surface for example, without producing a 'ringing' effect due to the (approaching) asymptotic walls of the beaker).

Table 5.1 Chemistry Beaker – 300ml true volume[1]

Mesh Size	Weight Parameters	Number of Data Points	Deformation Time (sec)	Number of Iterations	Volume Estimate (ml)	% Error
10x10	w_0=0.8 w_1=0.01 (stretchy)	944	11	250	290.6	3.1
10x10	w_0=0.0 w_1=0.5 (rigid)	944	11	250	223.1[2]	25.6
50x50	w_0=0.8 w_1=0.01 (stretchy)	944	60	250	307.1	2.4
50x50	w_0=0.0 w_1=0.5 (rigid)	944	60	250	329.1	9.7

[1]volume as measured using water displacement with graduated cylinder

[2]inaccuracy due to significant curling of the edges of the model due to its rigid nature

A second example is the volume estimate of a small specimen plastic chemistry dish. The dish was again placed face down on a flat surface for the experiment. The dish itself was square in shape with gradually sloping walls (in contrast with the steep walls of the beaker). Data were acquired for the dish in much the same way as for the beaker: defining an initial plane on the flat surface, outlining the outside of the dish and then finally digitizing the sides and shape of the dish. The volume estimate results for the plastic dish are presented in *Table 5.2.*

Table 5.2 Plastic Dish (outside) – 105ml true volume[3]

Mesh Size	Weight Parameters	Number of Data Points	Deformation Time (sec)	Number of Iterations	Volume Estimate (ml)	% Error
10x10	w_0=0.8 w_1=0.01 (stretchy)	660	8	250	112.4	7.0
10x10	w_0=0.0 w_1=0.5 (rigid)	660	8	250	106.8	1.7
50x50	w_0=0.8 w_1=0.01 (stretchy)	660	58	250	102.5	2.4
50x50	w_0=0.0 w_1=0.5 (rigid)	660	58	250	105.7	0.7

[3]volume as measured using water displacement with graduated cylinder

It is interesting to observe that configuring the model to be 'stretchy' was advantageous in obtaining an accurate volume estimate for the beaker due to the need for the model to conform to its steep walls while the 'rigid' surface produced a more accurate volume estimate for the dish due to its more gradual sloping walls. In any case, the volume estimates produced were reasonably representative of the actual volumes of these items. The 10x10 and 50x50 mesh sizes were chosen as extremes between which a likely mesh density will be chosen. Accordingly, the volume estimates obtained will lie between these in accuracy.

5.2 Phase II - Modelling Aspirator Suction for Tissue Resection

5.2.1 Experimental Procedure

The objective of the second phase of the validation studies was to investigate the ability of the deformable model to mimic tissue changes that occur when an aspirator device is used to resect tissue. A gelatin solution was used to model the consistency of the brain and an aspirator attachment to the FARO Surgicom was designed and constructed to reproduce the equipment setup (the CUSA) in the OR.

5.2.2 Construction of Biomechanical Phantoms

Biomechanical phantoms were constructed to mimic cerebral tissue in the aspirator simulator trials. Gelatin solutions of several concentrations were prepared (2% gelatin to 7% gelatin) and Dr. Abbas Sadikot, a neurosurgeon at the Montreal Neurological Institute, evaluated the resulting phantoms for their resemblance to the physical properties of actual cerebral tissue. He found that a biomechanical phantom constructed from a 3% gelatin (see *Figure 5.3*) solution quite accurately mimicked brain tissue.

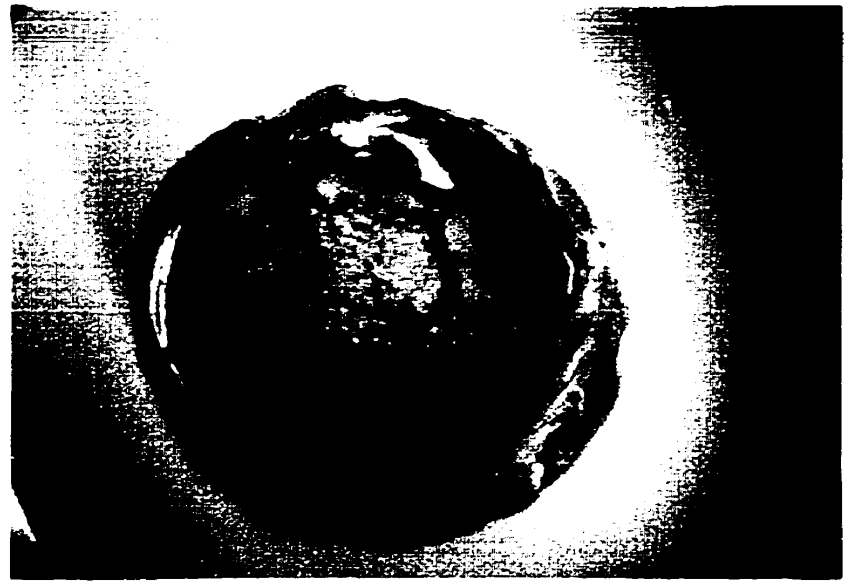

Figure 5.3 A biomechanical phantom made from 3% gelatin solution.

5.2.3 Construction of Aspirator Simulator

The device most often used in the operating room to resect cerebral tissue is the CUSA or aspirator. It is a suction device used by the surgeon to selectively remove tissue in small portions. In order to mimic the operation of the device and emulate its effects on tissue, a suitable substitute (the aspirator simulator) had to be constructed (the actual CUSA device was not immediately available to the author for use). The aspirator simulator was constructed as a thin hollow stainless steel rod affixed to aluminum shaft, which serves as the mount to the FARO Surgicom arm. One end of the hollow rod was connected to a sink-mounted water vacuum to produce the required suction. The aspirator simulator is shown in *Figure 5.4*. The aspirator simulator and its suction effect on the

gelatin biomechanical phantoms was validated with consultation from Dr. Abbas Sadikot. He found that the suction effect of the aspirator simulator on the gelatin phantoms closely mimicked the effects of the CUSA on cerebral tissue during a typical resection procedure.

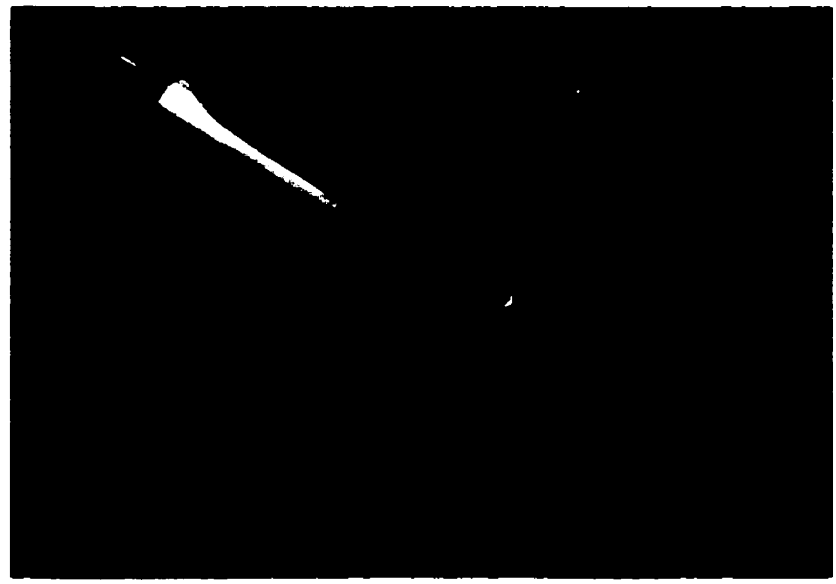

Figure 5.4 The aspirator simulator used in the validation studies. One end of the small hollow tube is connected to a water vacuum pump and the other end is used for suction. The hole in the aluminum shaft is for mounting to the FARO Surgicom probe holder.

5.2.4 Aspirator Simulator Tip Calibration Procedure

In order for the modelling software to track the position of the aspirator simulator tip using the FARO Surgicom, an accurate offset file (containing an affine transformation) must be produced to relate the position of the aspirator simulator tip to the probe holder mount of the FARO Surgicom. A method proposed by R. Comeau, a PhD candidate and fellow graduate student, was used to produce this offset file.

The calibration procedure was performed using a plastic circular disk containing an inner aluminum disk of radius r, along with the aspirator simulator connected to the FARO Surgicom (see *Figure 5.5*). Two holes (the same size as the hollow steel rod of the aspirator simulator) were drilled in the ends of the plastic disk along a chord corresponding to the diameter of the plastic circular disk. These holes were drilled from the outer edge of the plastic disk to the edge of the inner aluminum disk. With the plastic

and aluminum disk firmly affixed to a surface, the tip of the aspirator simulator was inserted fully into one of the holes and three data points were acquired at different rotations within the hole. The tip of the aspirator simulator was then inserted fully into the other hole and three additional data points were acquired. The three data points for each hole were used to determine the circles (and their centres) that the aspirator simulator circumscribes when being rotated in each of the holes. The algorithm for determining the centre of a circle given three points (a_x, a_y), (b_x, b_y) and (c_x, c_y) along its circumference is:

$$A = b_x - a_x \qquad B = b_y - a_y$$

$$C = c_x - a_x \qquad D = c_y - a_y$$

$$E = A(a_x + b_x) + B(a_y+b_y) \qquad F = C(a_x+c_x) + D(a_y+c_y)$$

$$G = 2(A(c_y-b_y) - B(c_x-b_x))$$

[5.1]

The centre of the circle P defined by these three acquired points is given by:

$$P = (p_x, p_y) \text{ where:}$$

$$p_x = (D \bullet E + B \bullet F) / G$$

$$p_y = (A \bullet F - C \bullet E) / G$$

[5.2]

In order to use the above algorithm, the FARO Surgicom must be oriented such that the three acquired points for each circle lie in a plane. This is accomplished without much difficulty due to the adjustments available on the arm.

Using the two centres of the circles determined above, a line segment connecting the two centres can be found, the midpoint of this line segment being the centre of the plastic disk and aluminum inner disk. By subtracting the radius of the inner aluminum disk, the coordinates of the aspirator simulator tip within each of the holes can be determined.

Since the aspirator simulator tip is axially symmetrical, one can assume that its orientation (ie. trajectory) is identical to the probe holder (ie. the holder to which the aspirator simulator is attached) points previously acquired. The points acquired are deemed to be in *probe base space* (with respect to the base of the FARO Surgicom). Therefore, a transformation is necessary to find the corresponding points with respect to the holder of the FARO Surgicom. In *probe holder space*, the tip of the aspirator simulator is always

located at the same vector offset to the probe holder origin since the coordinate reference frame rotates with the data points acquired with respect to the probe holder. Therefore, the coordinates of the aspirator tip in *probe holder space* are determined as:

$$TIP_{(x,y,z)}(holder\ space) = [T_{base}^{holder}] \bullet TIP_{(x,y,z)}(base\ space) \qquad [5.3]$$

The vector connecting the coordinate of the tip of the aspirator simulator in probe holder space to the origin of *probe holder space* (at the holder) constitutes the required offset file. This file is loaded in VIPER prior to using the aspirator simulator tip and FARO Surgicom to acquire data for deformation of the model.

Figure 5.5 The calibration apparatus used to generate the offset file for using the aspirator simulator with the FARO Surgicom. The plastic puck is held firmly in place with a clamp.

5.2.5 Modelling Capability

The basic modelling capabilities of the deformable model software were investigated in Phase I. In this phase the capability of the model to conform to a cavity dynamically created in a gelatin phantom with an aspirator simulator was investigated.

This task is somewhat different in that the aspirator simulator can suck or rip regions of the gelatin phantom when in use, creating small craters or dimples in the gelatin. Accurate acquisition of data representing the walls of the resection cavity was accomplished by touching the walls with the aspirator simulator tip after a piece of the gelatin was removed. Again, different parameter settings were used in this phase to determine optimal values for use in a typical neurosurgical procedure involving tissue resection. The results of a typical experiment involving the gelatin phantom and aspirator simulator are shown in *Figure 5.6*. Volume estimates obtained during these trials were typically within 5% of the actual volume of the cavities produced.

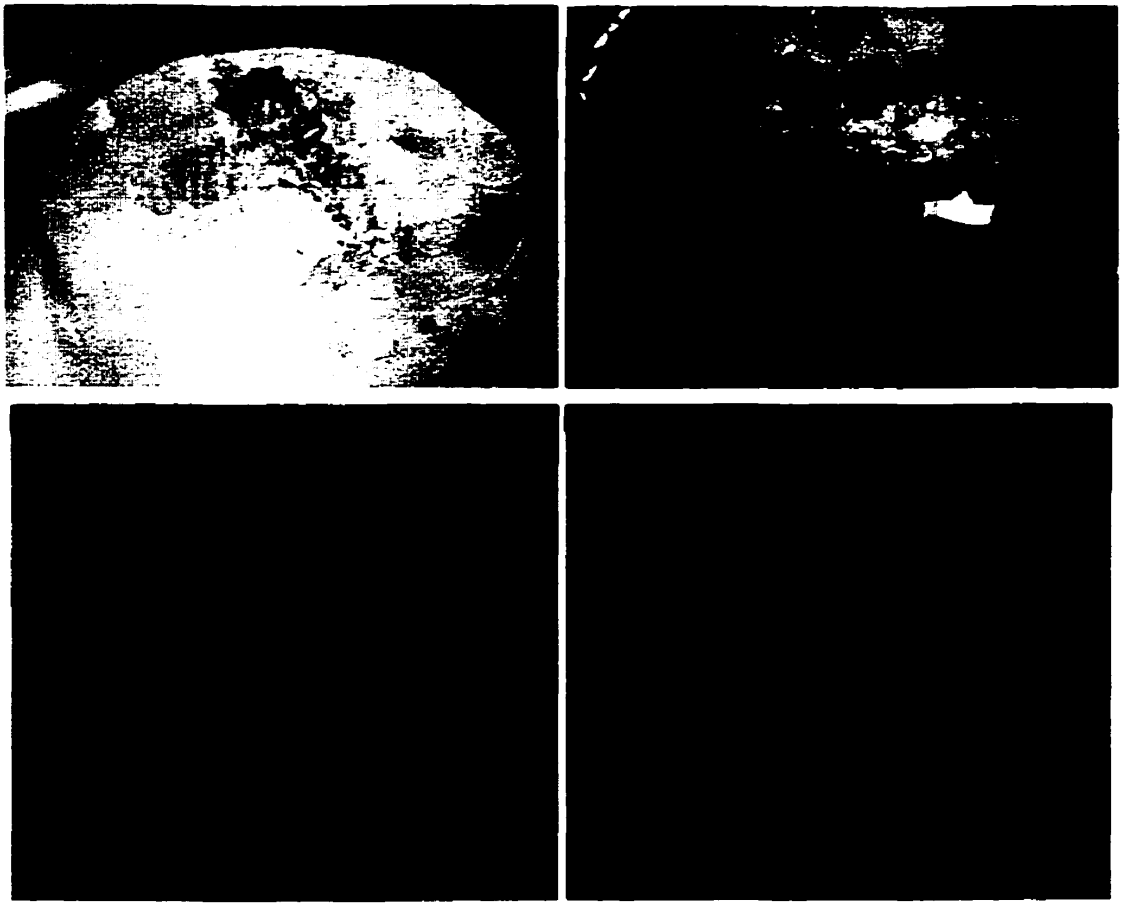

Figure 5.6 3% gelatin phantom with t-shaped cavity created with aspirator simulator. The photos above show the resection result on the phantom. Note the dimpling of the phantom created by the suction of the aspirator simulator. The lower images demonstrate the modelled result using a 50x50 mesh.

5.3 Phase III - Full Registration and Mock Resection Trials

5.3.1 Experimental Procedure

In the final phase of the validation study, a full mock resection with registration was performed. An MR compatible phantom was designed and constructed to allow for MR imaging of the gelatin biomechanical phantom and for subsequent registration purposes.

5.3.2 Construction of MR Phantom

The MR phantom was fabricated as a plexiglas cube containing a small box where the gelatin solution could be poured and set. The top outer corners of the cube have countersunk drill holes and one corner has an additional marker to resolve ambiguity in orientation when the MR data set is viewed within VIPER. The MR phantom is shown in *Figure 5.7.*

The gelatin biomechanical phantom contained within the inner box of the cube was constructed as follows. A 3% gelatin solution was prepared and allowed to cool before pouring into the inner box of the MR phantom. When the 3% gelatin solution had set, the aspirator simulator was used to create a cavity in the centre of the gelatin and a 3% gelatin solution doped with copper sulfate was prepared, allowed to cool, and then poured into the cavity. The copper sulfate doped gelatin would serve as the 'tumour' in the gelatin phantom, which would be resected using the software tracked aspirator simulator during the trial. The heterogeneous phantom produced possessed the properties of:

- cerebral tissue-like consistency and behavior when resected with the aspirator simulator
- a visual distinction between the 'tumour' (copper sulfate doped gelatin) and the normal tissue (regular gelatin)
- a visual distinction when imaged with a standard scan (12-15 min @ 1mm resolution) using a Siemens MR scanner (3D scan, TR=18ms, TE=10ms, tip angle = 30 degrees, 256x256x192 matrix, $1mm^3$ isotropic voxels)

The results of a MR scan of the MR phantom are shown as orthogonal slices *in Figure 5.8.*

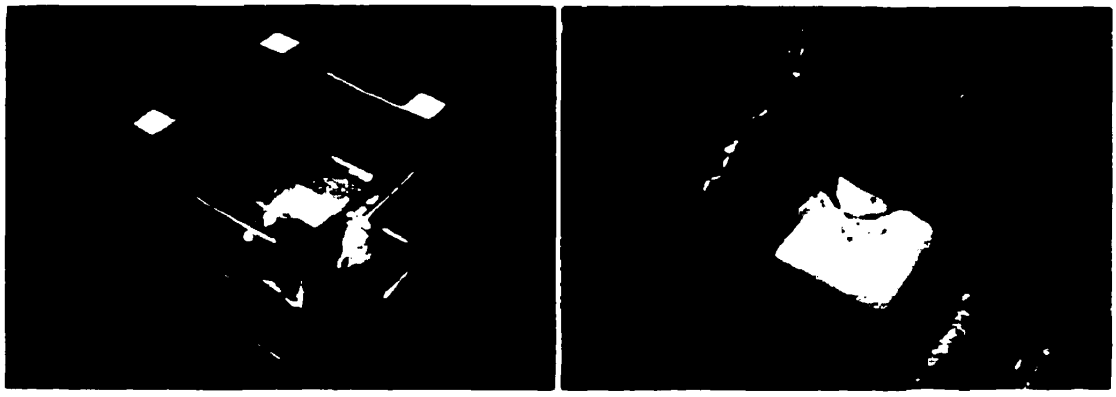

Figure 5.7 The MR phantom with inner box containing 3% gelatin solution used in Phase III validation study. The copper sulfate doped gelatin 'tumour' is seen at right in the centre of the box.

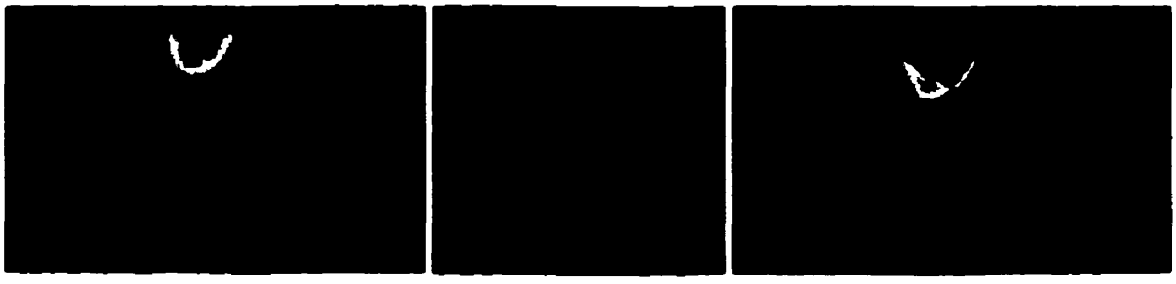

Figure 5.8 MR scan (orthogonal planes shown) of the MR gelatin phantom used in the Phase III validation study. Note the high contrast of the copper sulfate doped gelatin representing the 'tumour' relative to the regular gelatin (surrounding dark region).

5.3.3 Modelling Capability

The procedure for this phase of the validation study very closely followed the actions which would be performed during intraoperative use of the software. The

standard VIPER registration procedure was carried out to determine the correspondence between the MR phantom and the MR data set of phantom loaded in the VIPER software. Once the registration process was complete, an initial plane was defined with the aspirator simulator (after loading its offset file into VIPER) upon the top surface of the gelatin phantom. Resection of the copper sulfate doped gelatin 'tumour' was then performed using the aspirator simulator, acquiring data points as the resection progressed. At the conclusion of the mock resection procedure, some additional data points were acquired at the bottom of the resulting cavity and then the data points acquired during the procedure were saved to a file. The figures below illustrate the results of the resection procedure. The images in *Figure 5.9* are 3D reconstructions of the gelatin phantom with copper sulfate doped gelatin 'tumour' produced from the MR data set of the phantom. *Figure 5.10* depicts the deformable model result at the conclusion of the mock resection. The conformity between the gelatin tumour and the modelled result is illustrated in *Figure 5.11*. A view of the cross sections of the deformable model displayed in the 2D views of VIPER during an intermediate stage in the resection is shown in *Figure 5.12*. The volume estimation accuracy of the resulting cavity produced during the mock resection procedure was similar to that obtained in the earlier phases (within 5% of the true volume measured with water and graduated cylinder).

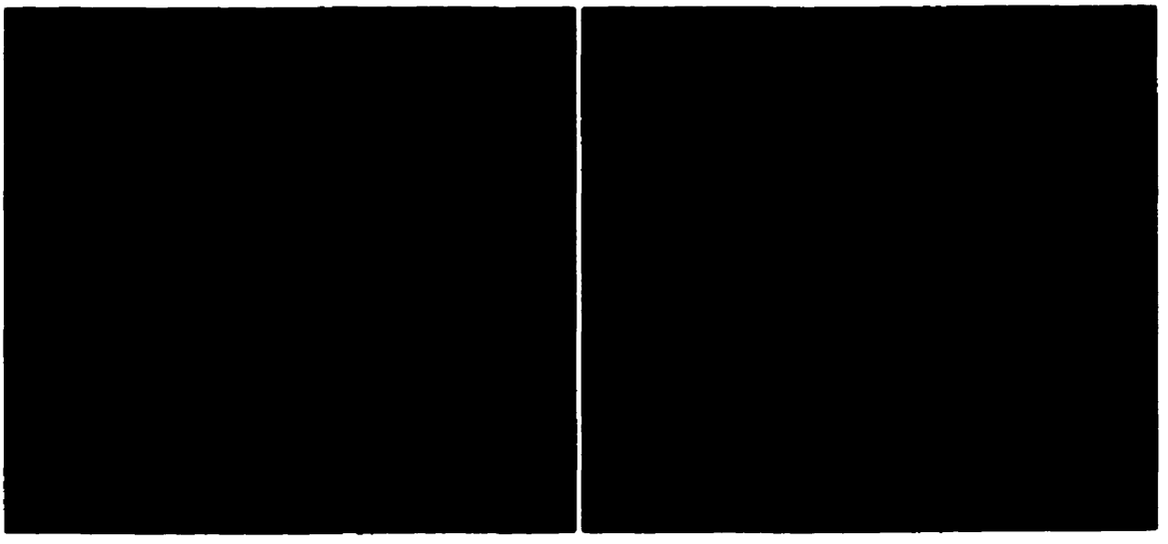

Figure 5.9 3D reconstruction of the gelatin phantom from its MR data set showing copper sulfate doped gelatin tumour.

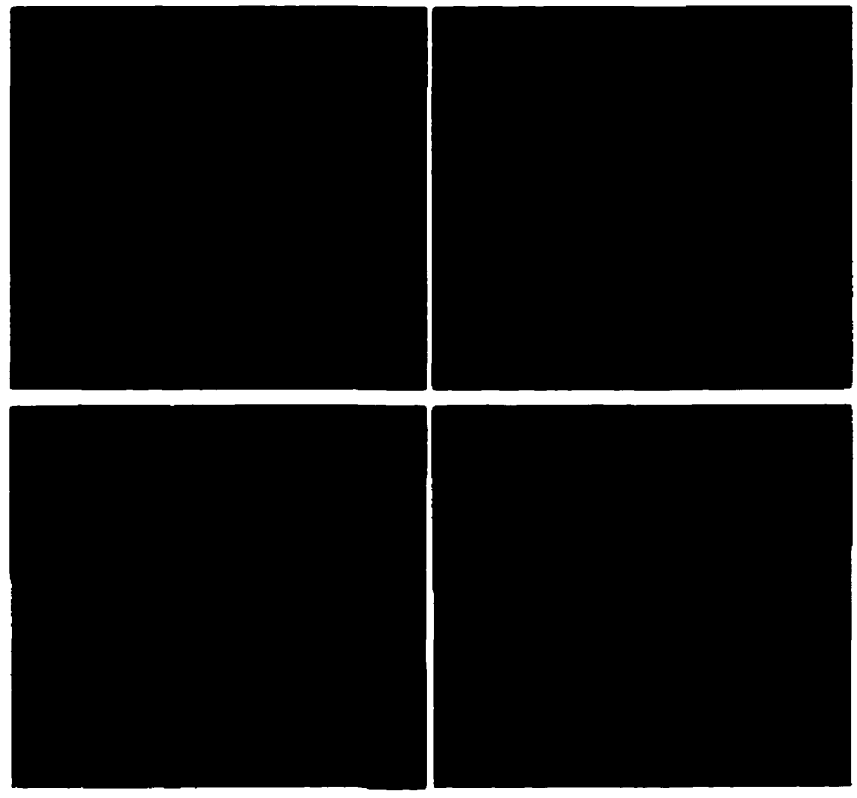

Figure 5.10 Renderings of the deformable model result from mock resection trial. The images above illustrate a translucently rendered model with visible data points. Note that most data points lie at the upper rim of the cavity or at the base of the cavity. The images below illustrate the opaquely rendered model result.

Figure 5.11 Various views of the deformable model result shown with the gelatin 'tumour'. Note the close conformance between the model and the resected tumour.

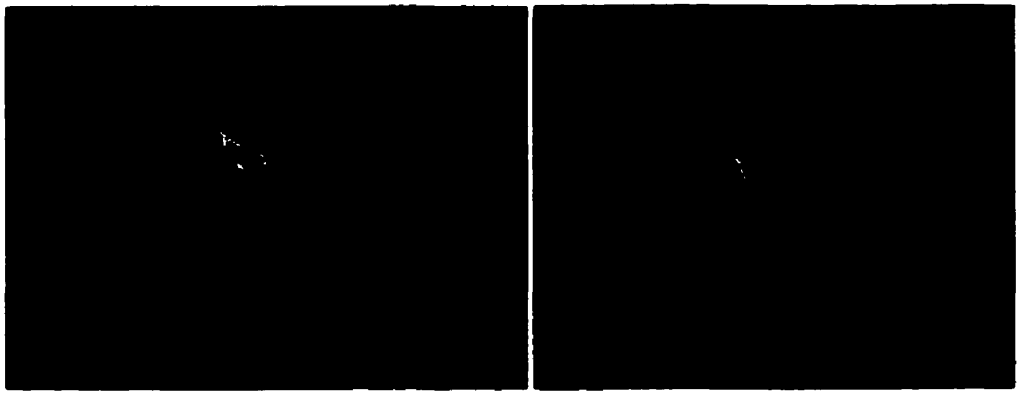

Figure 5.12 Various cross sections of the deformable model shown in VIPER's 2D views at an intermediate stage during the mock resection trial.

5.4 Conclusion

The purpose of the validation study undertaken was to determine the modelling and volume estimation capability of the software developed for this thesis. In Phase I, it was shown that the deformable model indeed has the capability of representing shapes with visual accuracy and good volume estimation accuracy. Phase II demonstrated that the model is capable of accomplishing the aforementioned tasks using a suction device very similar in action to the device (CUSA) often used in the OR. Phase III was designed to closely mimic the utility of the software when used in an intraoperative setting. This utility was borne out of the results achieved through the mock resection trial.

In conclusion, one can deduce that, through the results achieved during this validation study, that intraoperative feedback using the deformable model approach developed in this thesis is indeed a viable solution to the problem, both in terms of visual accuracy and volume estimation capability.

Chapter 6

Clinical Utilization

6.1 IGNS Environment in the Operating Room

In the IGNS environment in the OR, the use of the computer display of preoperative images and position tracking device serve as the surgeon's 'roadmap' in planning the trajectories to targets and guiding the surgical procedure. This section describes the typical course of a patient through the surgical process, from acquisition of preoperative images to postoperative assessment.

6.1.1 Preoperative Preparation

Approximately one week before the surgical procedure, a patient workup including imaging studies is performed. Typically MRI data is acquired to provide anatomical information and for differentiation of soft tissue (normal from pathological) and is the primary modality used for intraoperative surgical guidance, although CT is also sometimes used. Additional imaging studies are acquired as they are relevant to the procedure; vascular imaging such as MRA and DSA may be used in visualizing the cerebrovascular tree to relate the proximity of major vessels to the surgical site of interest. Functional imaging studies such as PET or fMRI may be warranted if the pathology lies close to an area of vital brain function. Electroencephalographic (EEG) recordings and cortical mappings may be made for resections relating to pharmacologically intractable epilepsy. In performing deep brain lesions for alleviation of Parkinson's Disease symptoms of tremors and rigidity [64], a brain atlas may be used to navigate deep brain structures. This procedure requires the computation of a non-linear transformation relating the MRI atlas model to the patient's MRI scan. Reformating and resampling of imaging data from different modalities is then performed to allow the different images to be superimposed in the IGNS environment. Segmentation of relevant objects from the patient's MRI data is

performed to create a polygonal representation of structures for the 3D view in the computer display.

6.1.2 Equipment Setup in the OR

Preparations for the surgical procedure begin as the anesthetisized is brought into the OR. The patient's shaved head is sterilized and rigidly fixed in the Mayfield clamp. The clamp itself is attached to the operating table with a series of mounts and adjustments are made. As this is occurring, the IGNS computer workstations are brought into the OR. The frameless IGNS system upon which the surgeon relies for guidance is the commercial, FDA approved ISG Viewing Wand (ISG Technologies, Mississauga, Ontario, Canada), which runs on an Hewlett-Packard workstation and uses the FARO Surgicom passive articulated arm as a position tracking device. Other experimental IGNS systems, such as VIPER (our laboratory's IGNS development platform) and MedViewer (an IGNS system also under development which merges intraoperative ultrasound with preoperative MRI data) are also regularly brought into the OR for validation and research purposes. These other systems share the position tracking data from the FARO Surgicom in order to do their own registrations and probe tracking. Imaging data sets are loaded into the Viewing Wand system via magnetic tape.

The FARO Surgicom is then secured to the Mayfield clamp (which fixes the patient's head) so that in the event that the patient's head must be moved during the surgery, the position tracking device will retain its relative position [11]. The position of the tip of the probe must be computed by the Viewing Wand software by inserting the tip into a hole at the base of the arm and sampling a few points at different angles [11]. After a check to determine if the range of maneuverability of the FARO arm is sufficient the registration is performed. This involves the calculation of the transformation matrix relating the patient space (physical space with respect to the patient) to the image space (the coordinate space of the preoperative images). The registration procedure is via the techniques discussed in Chapter 2; either by homologous point matching to fiducial markers on the frame (in a frame-based procedure) or anatomical points on the patient (in a frameless procedure) or by surface matching. A check of the accuracy of the resulting

registration is then performed by moving the probe around the outside of the patient's head and observing the corresponding position on the computer display. If the registration appears accurate, then the surgical procedure begins. Throughout the procedure, an OR technician is available to control the computer workstation and software at the request of the surgeon.

6.1.3 Postoperative Period

After a surgical procedure, it is common practice to acquire a follow-up MR scan to observe the results, particularly following a resection of tissue. Resection areas can be clearly seen to inspect whether or not the entire extent of the pathology has been removed. In the case of the creation of deep-seated lesions for thalamotomy and pallidotomy to improve symptoms of Parkinson's disease, the postoperative MR scan can be compared with a brain atlas [64]. Neurological examinations for functional deficits that may have occurred as a result of surgery are also performed in the postoperative period.

6.2 Neurosurgical Procedure Overview

In order to understand the complexity of the neurosurgeon's work and the utility of IGNS systems in their work, one must consider the constraints which must be considered that limit the options for surgical trajectory [65]:

- the skull – determination of the best location to perform a craniotomy for the trajectory chosen while at the same time avoiding excess bone removal
- the importance of tissue surrounding the surgical site of interest – traversing through the brain to a deep-seated lesion may pass through an area of functionally vital tissue, and this must be taken into consideration when planning a trajectory
- the fragility of brain tissue – the surgeon must avoid blood vessels that supply oxygen to the brain tissue to minimize the procedure's impact on healthy brain tissue

In addition, differentiation of pathological tissue from normal tissue by visual inspection is sometimes not possible [11], further complicating the surgeon's task. With these factors in mind, this section presents an overview of the general types of scenarios that confront

the surgeon to give a better understanding of the utility that the information provided by IGNS systems provide.

Although the intraoperative feedback provided by the project described here is primarily applicable to the resection of benign and malignant tumours and resections such as temporal lobectomies for intractable epilepsy, there exists a wide variety of situations that the surgeon may encounter for which IGNS systems are invaluable. The use of needle insertions into the brain for aspiration of cysts, biopsies of tissue and placement of depth electrodes can be aided by the guidance provided by a frame to accurately position the trajectory. Laser ablation of tissue exhibiting abnormal electroencephalographic activity and creation of deep-seated lesions in a thalomotomy or pallidotomy procedure can also benefit from IGNS guidance. Vascular imaging provided by IGNS systems can be of utility in surgical procedures to correct vascular abnormalities such as arterio-venous malformations (AVMs).

6.3 Clinical Utilization

The project described in this thesis was validated through experimental phantoms studies (as discussed in Chapter 5). While the clinical validation of the system was outside the intended scope of the project, this section therefore describes the proposed utility of the software in the intraoperative as well as the postpoperative period.

6.3.1 Intraoperative Usage

The utility of an IGNS environment to aid in the neurosurgeon's work has been elucidated in the previous chapters. The advantages and disadvantages of more sophisticated methods of intraoperative feedback were detailed in Chapter 1. The intent of the computer software developed for this project was to provide the neurosurgeon with visual feedback, as well as a quantitative volume estimate, of resections of benign and malignant tumours and resections of the temporal lobe for intractable epilepsy. The surgeon is able to define a plane (representing the deformable model in its initial state) in patient space using the probe (attached to the FARO arm) and when a resection is performed using an aspirator, data points are acquired to deform the model to visualize and calculate the volume of the

resection. This feedback is superimposed upon the preoperative images in the 2D and 3D views, provides the feedback using the existing IGNS environment (VIPER) and does not fundamentally alter the surgeon's work.

6.3.2 Postoperative Usage

In the postoperative period, the software allows for the data acquired during the surgical procedure and the preoperative images used as guidance during the procedure to be loaded into VIPER, enabling the surgeon to view an 'instant replay' of the resection that was recently performed. This feature can be used in concert with follow-up MR scans to determine if the full extent of the tumour has been removed.

Correlation of the extent of tissue resection with postoperative assessment of neurological deficit is another possible use of the intraoperative feedback provided by this project. During resection of regions such as the corpus callosum for treatment of intractable epilepsy, postoperative development of language disorders, neuropsychological impairment and motor dysfunction have been observed [66-68]. Attempts to correlate the extent of resection to the degree of impairment have been conducted [66,69,70] by tracing cross-sections of images from preoperative and postoperative scans. The feedback provided by the project has the capability of providing a volume estimate of the resection to aid in this process. This information can be used in conjunction with preoperative and postoperative neuropsychological testing to evaluate any degree of impairment of language, visual, motor, or cognitive impairment that has occurred as a result of the surgery.

Chapter 7

Conclusion and Future Work

7.1 Summary

The purpose of this thesis has been to present a case for the need for some sort of intraoperative feedback in the current IGNS system to account for changes in brain morphology and movement that may occur between the time preoperative imaging studies are undertaken and the time of surgery. The thesis details the design and implementation of a system providing intraoperative feedback using a typical IGNS environment. In Chapter 1 the motivation of the project was summarized. The typical IGNS environment was defined as a computer display of preoperative images, a position tracking device and associated computer software. Current alternatives to the project described in this thesis for providing intraoperative feedback were presented. The relevance of intraoperative feedback and the objectives of the projects were then presented. Chapter 2 served to familiarize the reader to the developments in neurosurgery that lead up to the current IGNS environment in use today. An overview of the use of different imaging modalities in the IGNS system was presented. Accuracy considerations in IGNS systems using preoperative images only were discussed to give the reader an appreciation of the limitations of these neuro-navigational systems.

A formal discussion of deformable models was presented in Chapter 3. An explanation of deformable models and the rationale for their use in this project was detailed. The mathematical development of the deformable model was elucidated, as was its numerical solution and algorithm implemented in computer software. The variables governing the behavior of the deformable model were discussed and the method implemented for computation of resection volume was described.

Full implementation details of the project were detailed in Chapter 4. The use of the software in the OR setting was described, along with the use of the FARO Surgicom, the connection of the aspirator to the probe and calibration of the aspirator tip. The

intraoperative feedback provided by the project within the context of VIPER and real-time interactivity issues were then presented.

The experimental studies used to tune the behavior of the deformable model and to validate its feasibility and efficacy in the visualization and quantification of cerebral tissue resection were presented in Chapter 5.

Chapter 6 presented a typical course of a patient through the neurosurgery process to provide the reader with an understanding of how IGNS systems are used for surgical planning and intraoperative guidance.

In conclusion, it is the author's belief that the objectives set forth in Chapter 1 have been met by the project described in this thesis. The use of deformable models for intraoperative feedback has the capability of providing useful visual and quantitative feedback to the neurosurgeon about the progress of tissue resection during a surgical procedure. In doing so, this information is provided using the equipment available in a typical IGNS environment, without the use of any specialized equipment and does indeed provide this feedback while simultaneously being unobtrusive to the surgeon's work.

7.2 Future Work

This section presents some possible extensions of the work presented in this thesis to ongoing IGNS related developments in our laboratory.

7.2.1 Use of functional imaging and probe tracking

One relatively simple extension of the project would be to construct 3D 'clouds' delineating functionally important areas from PET, fMRI, EEG, electrocorticography and stimulator tag points and then check the probe coordinates against these regions and alert the surgeon via an audible sound or a flashing display when the probe tip is close to these areas. These 'clouds' could also be displayed as translucent surfaces in the 3D view and as cross-sections in the 2D image display.

7.2.2 Extension of deformable model to accept data acquired from intraoperative ultrasound or laser rangefinder

The deformable model in this project was deformed using data points acquired from a probe point or an aspirator tip. An extension to this could involve the use of intraoperative ultrasound or a laser rangefinder as the data input to deform the model. This method of data acquisition would have the advantage of providing a large number of dense points in a short period of time, in contrast with the sparse number of data points gathered with the probe tip.

7.2.3 Integration of intraoperative feedback with intraoperative correction of brain movement and deformation for increased accuracy IGNS

The intraoperative feedback provided by this project can conceivably be coupled with current efforts in our laboratory for providing intraoperative correction of preoperative images when brain movement and deformation occur [2,3]. The superimposition of deformable modelling of tissue resection on intraoperatively corrected preoperative images would serve to provide a more accurate representation of the current state of the surgical field.

7.2.4 Integration of intraoperative feedback with volume-rendered multimodality display

Ongoing efforts in our laboratory to produce a stereoscopic volume rendered multimodality display [71] present another extension to the work presented in this thesis. At present, the deformable modelling of tissue resection can be displayed in a surface rendered 3D view or in cross-section in the 2D image views. The 3D view may be viewed stereoscopically as well. Presenting the extent of resection in a volume rendered display provides an additional option for representation of the cavity: a 'pixel-painting' approach. This method could conceivably 'colour in' the pixels corresponding to the resection cavity created. This type of approach would be extremely computationally expensive (ie. having to re-render the scene when the cavity is enlarged and more pixels are 'coloured in') but may be possible using parallel architectures or in the future with ever more powerful computational facilities.

Bibliography

[1] Vosburgh, K.G. "Image Guided Surgery and Its Potential", *Medicine Meets Virtual Reality*, K.S. Morgan et. al. (editors), IOS Press, 1997.

[2] Comeau, R.M., Fenster, A., and Peters, T.M. "Integrated MR and Ultrasound Imaging for Improved Image Guidance in Neurosurgery", *SPIE Proceedings on Medical Imaging*, K.M Hanson (editor), pp747-754, San Diego, California, 1998.

[3] Audette, M. "Brain Surface Motion Estimation and Tissue Modelling for Accurate Image Guided Neurosurgery and Surgical Simulation", MNI web page, URL: http://www.bic.mcgill.ca/research/groups/igns/fem/fem_michel/fem_home.html., March 1999.

[4] Lunsford, L.D. "A Dedicated CT system for the stereotactic operating room" *Appl. Neurophysiol.*, **45**, pp374-378, 1982.

[5] Lunsford, L.D. and Albright, L. "Intraoperative imaging with a therapeutic computed tomography scanner", *Neurosurgery*, **15**, pp559-561, 1984.

[6] Lunsford, L.D. et. al. "Stereotactic surgery using the therapeutic CT scanner", *Surg. Neurol.*, **18**, pp.116-122, 1982.

[7] Steinmeier, R. et. al. "Intraoperative Magnetic Resonance Imaging with the Magnetom Open Scanner: Concepts, Neurosurgical Indications and Procedures: A Preliminary Report", Deparment of Neurosurgery and Division of Neuroradiology, University of Erlangen-Nurnberg, and Siemens AG Medical Engineering, Erlangen, Germany, website, December 1998, URL: www.wwilkins.com/neurosurgery/full_text/0148-396X10-98p739.html.

[8] Steinmeier, R. et. al. "The Development and Implementation of Intraoperative MRI and its Neurosurgical Applications", Divisions of Neurosurgery and Neuroradiology, Brigham and Women's Hospital, Boston, MA, December 1998, URL: splweb.bwh.harvard.edu:8000/pages/papers/intra/intra.html.

[9] Galloway, R.L. and Maciunas, R.J. "Stereotactic Neurosurgery", *Critical Reviews in Biomedical Engineering*, **18**, 3, pp207-233, 1990.

[10] Henri, C. "Application of Stereoscopic Digital Subtraction Angiography to Stereotactic Neurosurgery Planning", Master's Thesis, Medical Physics Unit, McGill University, Montreal, Canada, 1989.

[11] Munger, P. "Accuracy Considerations in MR Image Guided Neurosurgery", Master's Thesis, Department of Physics, McGill University, Montreal, Canada, 1994.

[12] Galloway, R.L. et. al. "Interactive Image Guided Neurosurgery", *IEEE Trans. on Biomedical Engineering*, **39**, 12, December 1992.

[13] Vosburgh, K.G. "Image Guided Surgery and Its Potential", *Medicine Meets Virtual Reality*, K.S. Morgan et. al. (editors), IOS Press, 1997.

[14] Steinmeier, R. et. al. "The Development and Implementation of Intraoperative MRI and its Neurosurgical Applications", Divisions of Neurosurgery and Neuroradiology, Brigham and Women's Hospital, Boston, MA, December 1998, URL: splweb.bwh.harvard.edu:8000/pages/papers/intra/intra.html.

[15] Cosgrove, G.R. et. al. "Functional Magnetic Resonance Imaging for Intracranial Navigation", web-based research page, Departments of Neurosurgery and Radiology, Massachusetts General Hospital, Harvard Medical School, Boston, Massachusetts, December 1998, URL: neurosurgery.mgh.harvard.edu/frimage.htm.

[16] MacDonald, D. et. al. "Multiple Surface Identification and Matching in Magnetic Resonance Images", *Proc. 3rd Conf. Visual. in Biomed. Comp.*, Oct 4-7, 1994.

[17] Davey, B.L.K. et. al. "Multimodality Interactive Stereoscopic Image-Guided Neurosurgery", *VBC '94*, Montreal Neurological Institute, McGill University, Montreal, Canada and ISG Technologies, Mississauga, Canada, 1994.

[18] Davey, B.L.K. et. al. "Applying Stereoscopic Visualization to Image Guided Neurosurgery", Neuroimaging Laboratory, Montreal Neurological Institute, Montreal, Canada, ISG Technologies, Mississauga, Canada, and Departments of Neurology and Neurosurgery, McGill University, Montreal, Canada, 1994.

[19] Chandler, W.F. et. al. "Intraoperative Color Flow Doppler Imaging of AVMs and Aneurysms", *Journal of Neurosurgery*, **68**, pp635-639, 1998.

[20] FARO Technologies, Surgical Visualization, Localization and Navigation documentation, webpage material, www.faro.com, Mary Lake, Florida, USA, December 1998.

[21] BrainLAB GmbH, Image Guided Surgery documentation, webpage material, www.brainlab.com, Germany, December 1998.

[22] BrainLAB GmbH, VectorVision Surgical Tracking System paper documentation, Germany, October 1997.

[23] Northern Digital Inc., 3D Optical Measurement Equipment – OPTOTrack System, webpage material, www.ndigital.com, Waterloo, Ontario, Canada, December 1998.

[24] Maurer, C.R. et. al. "The accuracy of image guided neurosurgery using implantable fiducial markers", *Computer Assisted Radiology 1995*, pp1197-1202, Springer-Verlag, Berlin, 1995.

[25] Colchester, A.C.F. et. al. "Development and preliminary evaluation of VISLAN, a surgical planning and guidance system using intraoperative video imaging" ***Med. Image Analysis*, 1**, pp73-90, 1996.

[26] Roberts, D.W. et. al. "A frameless stereotaxic integration of computerized tomographic imaging and the operating microscope" *J. Neurosurgery*, **65**, pp545-549, 1986.

[27] Kato, A. et. al. "A frameless, armless navigational system for computer assisted neurosurgery", Technical Note, *Journal of Neurosurgery*, **74**, 5, pp845-849, May 1991.

[28] Hill, D.L.G. et. al. "Estimation of Intraoperative Brain Surface Movement", UMDS, Guy's and St. Thomas' Hospital, London, UK, Vanderbilt University, Nashville, TN, USA, 1997.

[29] Munger, P. et. al. "Registration Error in MR Based Image Guided Neurosurgery", Montreal Neurological Institute, *COMP '95*, 1995.

[30] Comeau, R. "Intraoperative Ultrasound in Interactive Image Guided Neurosurgery", web page, URL: www.bic.mni.mcgill.ca/research/groups/igns/US/us_home.html, December 1998.

[31] McInerney, T. and Terzopoulos, D. "Deformable Models in Medical Image Analysis: A Survey", *Medical Image Analysis*, **1**, 2, 1996.

[32] Terzopoulos, D. and McInerney, T. " Deformable Models and the Analysis of Medical Images", *Medicine Meets Virtual Reality*, IOS Press, 1997.

[33] Foley et. al. *Computer Graphics: Principles and Practice*, Addison-Wesley Publishing Co., New York, 1993.

[34] Terzopoulos, D. and Qin, H. "Dynamic NURBs with Geometric Constraints for Interactive Sculpting", *ACM Trans. on Graphics*, **13**, 2, pp103-136, April 1994.

[35] Sethian, J.A. et. al. "Shape Modelling with Front Propagation: A Level Set Approach", *IEEE Trans. Patt. Anal. and Mach. Intel.*, **17**, 2, pp158-174, February 1995.

[36] Adalsteinsson, D. and Sethian, J.A. "A Fast Level Set Method for Propagating Interfaces", *Journal of Computational Physics*, **118**, pp269-277, 1995.

[37] Osher, S. and Sethian, J.A. "Fronts Propagating with Curvature Dependent Speed: Algorithms Based on Hamiltonian-Jacobi Formulations", *Journal of Computational Physics*, **79**, pp12-49, 1998.

[38] Pentland, A. "Automatic Extraction of Deformable Part Models", International *Journal of Computer Vision*, **4**, pp107-126, 1990.

[39] Pentland, A. "Canonical Fitting of Deformable Part Models", *SPIE, 1260, Sensing and Reconstruction of Three Dimensional Objects and Scenes*, 1990.

[40] Sclaroff, S. and Pentland, A. "Modal Matching for Correspondence and Recognition", *MIT Media Laboratory Perceptual Computing Section Technical Report no. 201*, May 1993.

[41] Pentland, A. and Sclaroff, S. "Closed form Solutions for Physically Based Shape Modelling and Recognition", *IEEE Trans. Patt. Anal. and Mach. Intel.*, **13**, 7, July 1991.

[42] Pentland, A. and Horowitz, B. "Recovery of Nonrigid Motion and Structure", *IEEE Trans. Patt. Anal. and Mach. Intel.*, **13**, 7, 1991.

[43] Martin, J., Pentland, A. et. al. "Shape Analysis of Brain Structures Using Physical and Experimental Modes", *MIT Media Laboratory Perceptual Computing Technical Report no. 276*, January 1994.

[44] Cohen, I. and Cohen, L.D. "A Hybrid Hyuperquadric Model for 2D and 3D Data Fitting", *CVGIP: Computer Vision and Image Understanding*, **63**, 3, pp527-541, 1996.

[45] Cohen, L.D. and Cohen, I. "Finite Element Methods for Active Contour Models and Balloons for 2D and 3D Images", *IEEE Trans. on Patt. Analysis and Mach. Intel.*, **15**, 11, pp1131-1147, November 1993.

[45] Miga, M. "Development and Quantification of a 3D Brain Deformation Model Experiencing Comparable Surgical Loads", PhD proposal, Thayer School of Engineering, Dartmouth College, Hanover, HH, USA, August 1997.

[47] Bro-Nielson, M. and Cotin, S. "Real Time Volumetric Deformable Models for Surgery Simulation using Finite Elements and Condensation", Institute of Mathematical Modelling, Technical University of Denmark, 1996.

[48] Bro-Nielson, M. "Modelling Elasticity in Solids using Active Cubes – Application to Simulated Operations", Institute of Mathematical Modelling, Technical University of Denmark, 1996.

[49] Bro-Nielson, M. "Active Nets and Cubes", Institute of Mathematical Modelling, Technical University of Denmark, 1994.

[50] Bro-Nielson, M. "Fast Finite Elements for Surgery Simulation", *Medicine Meets Virtual Reality*, K.S. Morgan et. al. (editors), IOS Press, 1997.

[51] McInerney, T. and Terzopoulos, D. " Finite Element Techniques for Fitting a Deformable Model to 3D Data", obtained directly from author (unpublished), University of Toronto, Toronto, Canada, 1994.

[52] Terzopoulos, D. et. al. "Elastically Deformable Models", *Computer Graphics*, **21**, 4, July 1987.

[53] Barr, A. "Superquadrics and Angle Preserving Transformations", *IEEE Computer Graphics and Applications*, **18**, 1981.

[54] Terzopoulos, D. and Metaxas, D. "Dynamic 3D Models with Local and Global Deformations: Deformable Superquadrics", *IEEE Transactions on Pattern Analysis and Machine Intelligence*, **13**, 7, July 1991.

[55] Metaxas, D. and Terzopoulos, D. "Constrained Deformable Superquadrics and Nonrigid Motion Tracking", *1991 IEEE Computer Society Conference on Computer Vision Proceedings*, 1991.

[56] McInerney, T. and Terzopoulos, D. "A Dynamic Finite Element Surface Model for Segmentation and Tracking in Multidimensional Medical Images with Application to Cardiac 4D Image Analysis", *Journal of Computerized Medical Imaging and Graphics*, 1994.

[57] Nastar, C. and Ayache, N. "Frequency Based Non-rigid Motion Analysis: Application to Four Dimensional Medical Images", *IEEE Trans. Patt. Anal. and Mach. Intel.*, **18**, 11, pp1067-1079, November 1996.

[58] McInerney, T.J. "Topologically Adaptable Deformable Models for Medical Image Analysis", PhD Thesis, Department of Computer Science, University of Toronto, 1994.

[59] McInerney, T.J. and Terzopoulos, D. "Topologically Adaptable Snakes", *Fifth International Conference on Computer Vision (ICCV '95)*, pp840-845, June 1995.

[60] McInerney, T. and Terzopoulos, D. "Medical Image Segmentation using Topologically Adaptable Surfaces", obtained directed from author, 1994.

[61] Press, W.H. *et. al. Numerical Recipes in C*, Cambridge University Press, New York, 1992.

[62] Cook, L.T. et. al. "An Algorithm for Volume Estimation Based on Polyhedral Approximation", *IEEE Trans. on Biomedical Engineering*, **27**, 9, pp493-499, September 1980.

[63] Eberly, D. et. al. "On Gray Scale Measurements: II. Surface Area and Volume", *CVGIP: Graphical Models and Image Processing*, **53**, 6, pp550-562, November 1991.

[64] St. Jean, P. "Computer Guidance in Thalamotomy and Pallidotomy", Master's Thesis, Medical Physics Unit, McGill University, 1997.

[65] Galloway, R.L. et. al. "Interactive Image Guided Neurosurgery", *IEEE Trans. on Biomedical Engineering*, **39**, 12, December 1992.

[66] Mamelak, A.N. et. al. "Corpus callosotomy: a quantitative study of the extent of resection, seizure control and neuropsychological outcome", *Journal of Neurosurgery*, **79**, pp688-695, 1993.

[67] Gazzaniga, M.S. et. al. "Psychologic and Neurologic Consequences of Partial and Complete Cerebral Commisurotomy", *Neurology*, **25**, pp10-15, 1975.

[68] Gazzaniga, M.S. et. al. "Language After Section of the Cerebral Commisures, *Brain*, **90**, pp131-148, 1967.

[69] Davies, K.G. et. al. "Language Function After Temporal Lobectomy Without Stimulation Mapping of Cortical Function", *Epilepsia*, **36**, 2, pp130-136, 1995.

[70] Trenerry, M.R. et. al. "MRI Hippocampal Volumes and Memory Function Before and After Temporal Lobectomy", *Neurology*, **43**, pp1801-1805, September 1993.

[71] St. Jean, P., Sadikot, A.F., et. al. "Automated Atlas Integration and Interactive Three Dimensional Visualization Tools for Planning and Guidance in Functional Neurosurgery", *IEEE Trans. on Medical Imaging*, **17**, 5, October 1998.